OXFORD

Human Molecular Genetics, 2016, Vol. 25, No. 8 1501–1516

doi: 10.1093/hmg/ddw029
Advance Access Publication Date: 7 February 2016
Original Article

ORIGINAL ARTICLE

NLRP3 inflammasome activation drives bystander cone photoreceptor cell death in a P23H rhodopsin model of retinal degeneration

Ishaq A. Viringipurampeer, Andrew L. Metcalfe, Abu E. Bashar, Olena Sivak, Anat Yanai, Zeinabsadat Mohammadi, Orson L. Moritz, Cheryl Y. Gregory-Evans and Kevin Gregory-Evans*

Department of Ophthalmology and Visual Sciences, University of British Columbia, 2550 Willow Street, Vancouver, BC, Canada V5Z 3N9

*To whom correspondence should be addressed. Tel: +1 6048755525; Fax: +1 6048754663; Email: kge30@mail.ubc.ca

Abstract

The molecular signaling leading to cell death in hereditary neurological diseases such as retinal degeneration is incompletely understood. Previous neuroprotective studies have focused on apoptotic pathways; however, incomplete suppression of cell death with apoptosis inhibitors suggests that other mechanisms are at play. Here, we report that different signaling pathways are activated in rod and cone photoreceptors in the P23H rhodopsin mutant rat, a model representing one of the commonest forms of retinal degeneration. Up-regulation of the RIP1/RIP3/DRP1 axis and markedly improved survival with necrostatin-1 treatment highlighted necroptosis as a major cell-death pathway in degenerating rod photoreceptors. Conversely, up-regulation of NLRP3 and caspase-1, expression of mature IL-1β and IL-18 and improved cell survival with *N*-acetylcysteine treatment suggested that inflammasome activation and pyroptosis was the major cause of cone cell death. This was confirmed by generation of the P23H mutation on an *Nlrp3*-deficient background, which preserved cone viability. Furthermore, Brilliant Blue G treatment inhibited inflammasome activation, indicating that the 'bystander cell death' phenomenon was mediated through the P2RX7 cell-surface receptor. Here, we identify a new pathway in cones for bystander cell death, a phenomenon important in development and disease in many biological systems. In other retinal degeneration models different cell-death pathways are activated, which suggests that the particular pathways that are triggered are to some extent genotype-specific. This also implies that neuroprotective strategies to limit retinal degeneration need to be customized; thus, different combinations of inhibitors will be needed to target the specific pathways in any given disease.

Introduction

The mammalian retina is one of the most intensively studied parts of the central nervous system both from the perspective of understanding common blinding diseases, and also as a relatively accessible model system for neurodegeneration. The phototransduction protein rhodopsin is the most abundant protein in the retina (1). It is synthesized in rod photoreceptor endoplasmic reticulum (ER), and after post-translational modification and proper folding it is transported via the Golgi to the rod photoreceptor outer segment (2). Mutations in the rhodopsin gene are the most frequent cause of autosomal dominant retinitis pigmentosa (adRP) (3), a condition where patients exhibit night blindness and tunnel vision followed by a progressive loss of central vision due to the loss of cone photoreceptors (4). The P23H mutation accounts for ~12% of adRP in the USA (5). To date though, it is still unclear why rod photoreceptors die in

Received: November 16, 2015. **Revised:** January 21, 2016. **Accepted:** February 1, 2016

patients with rhodopsin mutations and even more thought-provoking, why genetically normal cone photoreceptors that do not express rhodopsin also die.

A number of pathways are brought into play when a genetic mutation leads to cell death. These may be subdivided into early and late events. Early events in the P23H model include misfolded protein accumulation and ER stress (6,7), whereas late events include programed cell-death responses such as caspase-dependent and -independent apoptosis (8). Recent studies in other rhodopsin mutants (T17M and E349X) show significant up-regulation of pro-inflammatory markers associated with an ER-stress response (9), but this has yet to be examined in the P23H mutant. The NLRP3 inflammasome is a crucial component of the innate immune system that is traditionally activated by a variety of stress-associated signals such as pathogens, metabolic defects, trauma and RNA/DNA damage (10–12) ultimately leading to pyroptotic cell death (13). These external and internal signals result in activation of NLRP3 either through the NF-κB pathway via Toll-like receptor activation or by the production of reactive oxygen species (ROS) (13). Activation of the inflammasome is reported to be a two-stage process requiring a priming event to up-regulate NLRP3-gene expression (14) and then the secondary assembly of a cytoplasmic multiprotein complex (NLRP3/ASC/Casp1). This is responsible for the maturation and secretion of pro-inflammatory cytokines IL-1β and IL-18 (15,16). Although inflammasome activation via Toll-like receptors is well-understood, activation of the NLRP3 inflammasome, via release of ROS from mitochondria is less well-characterized (11). In particular, the upstream signals that lead to ROS release are largely unknown. One recently proposed candidate is cell-death regulator RIP3 that has not only been shown to trigger ROS release (17,18), but also to activate the inflammasome (19). Although these experiments have highlighted a potential mechanism for RIP3 to activate the inflammasome in cell culture this has yet to be established as a mechanism *in vivo* in diseased tissue.

In this study, we investigated late cell-death signaling and pro-inflammatory pathways in the P23H-1 model of retinal degeneration. We report that rod photoreceptors die by necroptosis via an RIP1/RIP3/DRP1 mechanism. Conversely, bystander cell death (20) in genetically normal cone photoreceptors is mediated via NLRP3 inflammasome activation. We, therefore, propose that combinatorial neuroprotection strategies aimed at these two distinct pathways represents a new therapeutic approach for the treatment of P23H retinitis pigmentosa (RP).

Results

Delineation of cell-death pathways activated in P23H-1 retina

Progressive photoreceptor degeneration in the retina of the P23H-1 strain begins at about P15 when the eyes open and was assessed up to postnatal day (P) 120 where only 3–4 rows of photoreceptor nuclei remained in the outer nuclear layer (ONL) of the retina (Fig. 1A–D). Significant numbers of Terminal deoxynucleotidyl transferase dUTP nick end labeling (TUNEL)-positive cells were seen in the ONL in P23H-1 retina at P15 (286 ± 16 cells/mm^2) with a reduced number at P21, P45 and P120 (118 ± 11, 65 ± 5 and 52 ± 6 cells/mm^2, respectively), suggesting that cell death mostly occurred at the earlier stages of the degenerative process (Fig. 1E–H). To determine which cell-death pathways were triggered during the most active phase of retinal degeneration, we tested the expression of a number of cell-death markers. Activated caspase-3 (aCasp3) was present in a few photoreceptor nuclei in the degenerating retina from P15 to P120 suggesting caspase-dependent apoptosis was occurring in a limited number of cells throughout the degenerative process (Fig. 1I–L), in agreement with other studies in the P23H-1 model (8,21). Seeing aCasp3-positive material in the outer plexiform layer (Fig. 1L) most likely represents cellular debris migrating to the retinal vasculature for disposal (22). Poly ADP ribose polymerase (PARP), which is a marker of caspase-independent apoptosis, was also detected in the mutant P23H-1 retina (Fig. 1M–P). At P21, PARP was mostly present in the inner nuclear layer (INL) and ganglion cell layers of the retina (Fig. 1N), which do not contain the dying photoreceptor cells. Only a few photoreceptor cells in the ONL expressed PARP (Fig. 1N and O), consistent with previous reports showing that expression of PARP was not significantly elevated in the P23H-1 model (8). To determine if the necroptosis cell-death pathway was activated in P23H-1 retinal degeneration the expression of RIP1 and RIP3 proteins was also investigated. A high level of RIP1 expression was observed in both degenerating rods and cones at P120 compared with wild-type (WT) (Fig. 2A and B), whereas RIP3 was specifically expressed in rod photoreceptors at P21 and P120 (Fig. 2D and F), but not in cone photoreceptors (Fig. 2E). Relative to WT retinal extracts western blotting in P23H-1 retinal extracts revealed a 5- and 15-fold increase of RIP1 expression at P45 and P120, respectively (Fig. 2G). Similarly, RIP3 expression was highly up-regulated in P23H-1 retina compared with WT controls (Fig. 2H). No significant changes in the expression or cleavage of the autophagic vacuole marker LC3 was observed (Fig. 2I), suggesting that autophagy was not activated (23,24). Collectively, these results show activity of a number of different cell-death pathways in the degenerating P23H-1 retina.

Cell death in rod photoreceptors

High levels of RIP1 and RIP3 expression suggested that necroptosis may be the principal active pathway in rod photoreceptors. In support of this, lactate dehydrogenase (LDH) levels in vitreous gel of the eye were measured (as a surrogate for measuring levels in the extracellular space), since it has been shown that extracellular LDH increases during necrosis as cells become porous when they die (25). In keeping with previous studies (26), we found a dramatic increase in LDH levels in P23H-1 vitreous at P120 (Fig. 2J), suggesting that necroptosis is indeed occurring in P23H-1 degenerating retina.

We investigated the expression of RIP3 and dynamin-related protein 1 (DRP1) in the retina since assembly of the RIP1-RIP3 complex activates the GTPase DRP1 leading to its dephosphorylation and translocation into the mitochondria (27). DRP1 expression in P23H-1 whole retinal extracts was increased 2- to 3-fold over WT levels at P45 and P120 (Fig. 3A). However, in the mitochondrial fraction of the P23H-1 retinal extracts, RIP3 was elevated 3- to 6-fold (Fig. 3B) and DRP1 was elevated 4-fold (Fig. 3C), with only minimal levels detected in the WT mitochondrial fractions. This confirmed DRP1 translocation into the mitochondria. The expression of PGAM5 was also examined since the mitochondrial phosphatase PGAM5 is a substrate for RIP3 and this enzyme complexes with RIP1/RIP3/MLKL in the necrosome (27). Low levels of PGAM5 were present in the retinal mitochondrial fraction of WT eyes whereas we found a 5- to 10-fold increase in PGAM5 in P23H-1 retina (Fig. 3C). We also found that total mitochondrial protein was reduced by 30% reflecting loss of mitochondria through fission and fragmentation. Immunohistochemistry (IHC) demonstrated ubiquitous low-level DRP1 staining in the inner and outer segments of WT photoreceptors. In P23H-1 retina, DRP1 staining appeared to be preferentially elevated at the inner/outer segment boundary of rod

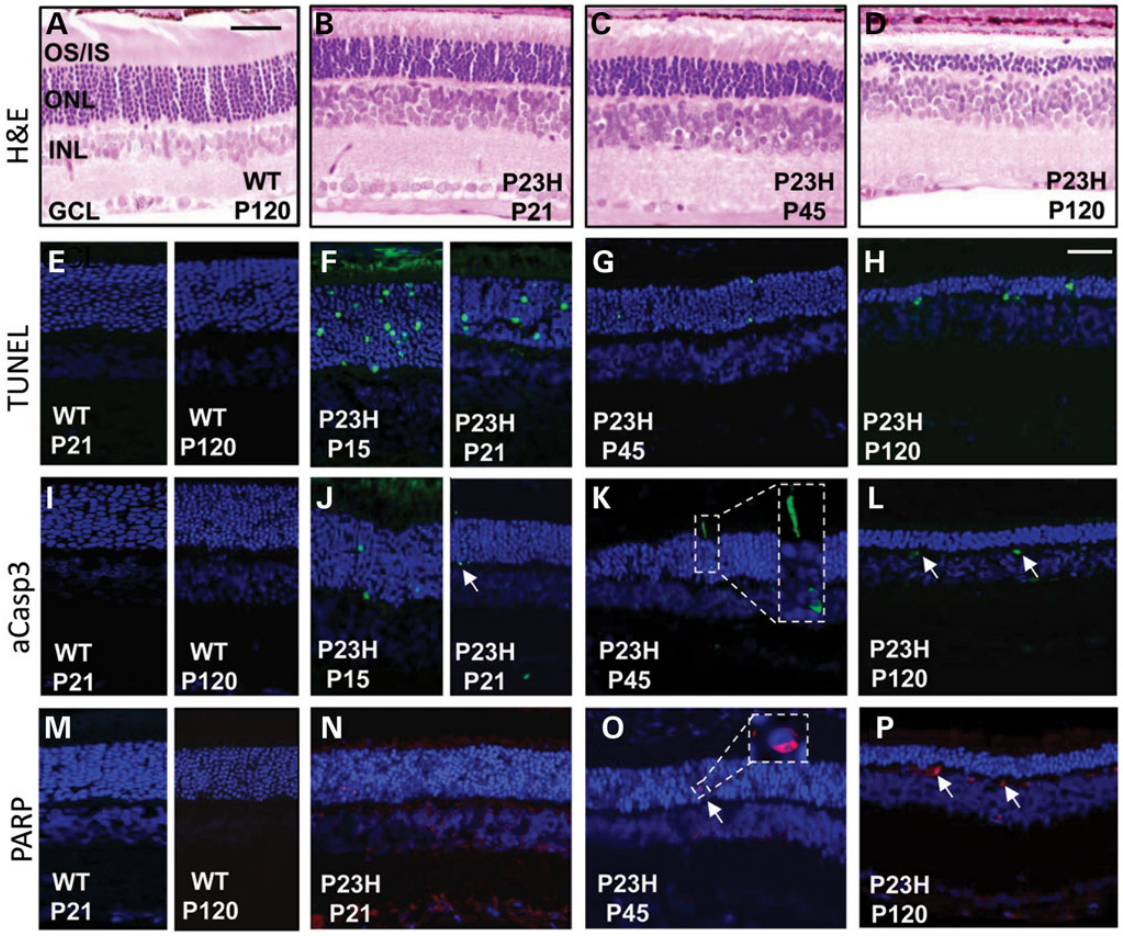

Figure 1. Active cell-death pathways in P23H retina. Representative images are shown from the eyes of each of six animals per age group ($n = 12$) that were tested with all antibodies from two independent experiments. (**A–D**) H&E stained sagittal sections through WT and P23H retina at postnatal days (P) 21, P45 and P120. OS/IS, photoreceptor outer segment/inner segment layer; ONL, photoreceptor outer nuclear layer; INL, inner nuclear layer; GCL, ganglion cell layer. Scale bar in (A) = 50 µm. (**E–H**) Retinal sections showing photoreceptor nuclei undergoing cell death by TUNEL staining (green). Nuclei counterstained with DAPI. Scale bar in (H) = 25 µm and represents the image size in all confocal sections. (**I–L**) aCasp3 labeling (green). (K) Inset shows aCasp3 in photoreceptor nuclei and in the inner segment of a photoreceptor. Arrows, aCasp3-positive cells. (L) Arrows denote cells in the outer plexiform layer of the retina. (**M–P**) PARP staining (red) in retina sections. (O) Inset shows PARP labeling in a single nucleus. (P) Arrows, PARP-positive cells in outer plexiform layer of the retina.

photoreceptors, whereas low levels of DRP1 co-localized with cone photoreceptors (Fig. 3D), because the unphosphorylated from of DRP1 is ubiquitously expressed.

Cell death in cone photoreceptors

Previous work has suggested that inflammatory cytokines are up-regulated in rhodopsin mutant retina (9). Active caspase-1 is known to play a role in the maturation of IL-1β and IL-18 precursors. In P23H-1, retinal extracts both of these mature, pro-inflammatory cytokines could be detected whereas only their precursors were present in WT retinal extracts (Fig. 3E). To determine if activation of the inflammasome was the cause of increased retinal cytokines, we examined the expression of NLRP3 and cleaved caspase-1. Both of these proteins were detected in the inner segments of mutant photoreceptors (Fig. 4B and D). On further analysis, intracellular NLRP3 expression was detected in cone photoreceptors cells that were identified with an extracellular marker [peanut agglutinin (PNA)] that detects the cone matrix sheath of the inner and outer segments (Fig. 4F). NLRP3 did not label the inner segments of rod photoreceptors (Fig. 4H). In addition, a low level of NLRP3 expression could be seen in the INL of the retina suggesting inflammasome activation in non-photoreceptor cell types (Fig. 4H), possibly reflecting previously reported cone bipolar cell loss in retinal degeneration (28,29). Western blot (WB) analysis confirmed the presence of NLRP3 in P23H-1 retina, whereas this protein was undetectable in WT retinal extracts (Fig. 4G). Pro-caspase-1 (pCasp1) was present at low levels in WT retina extracts, but was present at a 10-fold higher level in P23H-1 retina. The active, cleaved from of caspase-1 however was only present in P23H-1 retina extract (Fig. 4G).

Inflammasome activity in other retinal cells

Microglia are the main source of localized, innate immunity in the CNS and retina where they are actively recruited to release IL-1β into damaged tissue (30,31). IHC using microglial surface marker Iba1 showed that a few resident microglia could be identified in the inner retina of WT retina at P120 (Fig. 5A), in comparison with P23H-1 retina which showed increased numbers of microglia that were recruited to and migrating through the retina to the photoreceptor layer (Fig. 5B). Whole-mount retinal staining for Iba1 showed numerous microglia in P23H-1 retina, but very few in WT retina (Fig. 5D and E). We also identified Cd11b surface

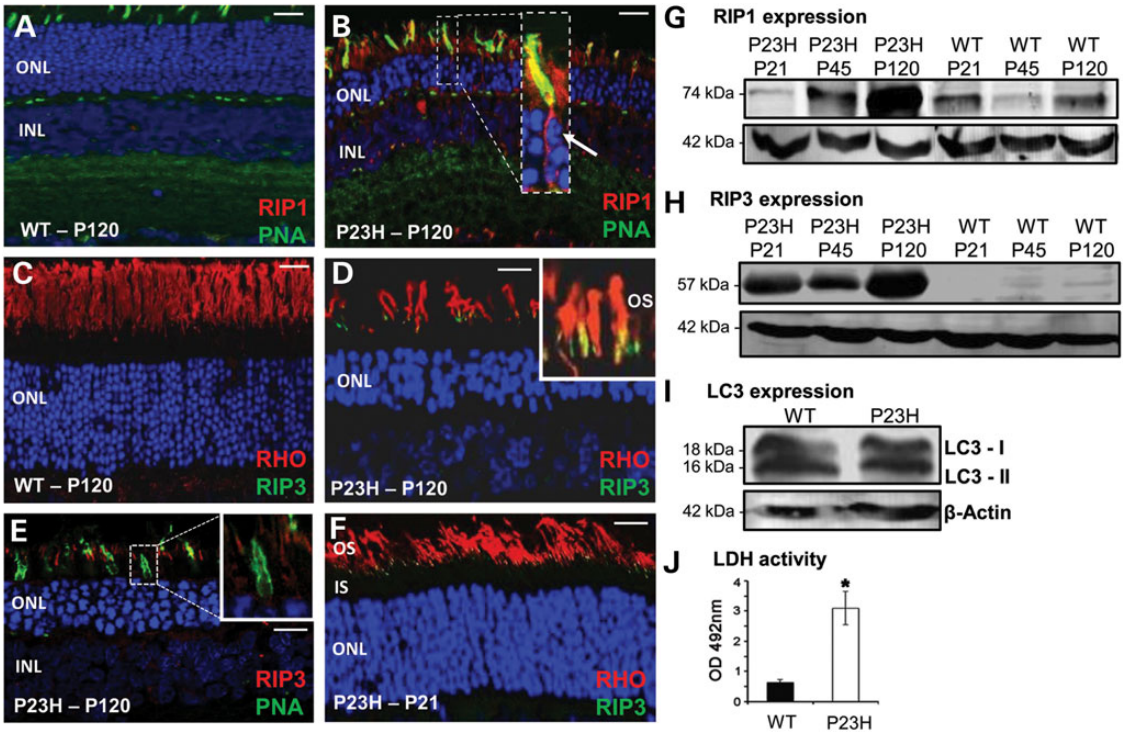

Figure 2. Expression of necroptosis and autophagy markers in WT and P23H rat retina. (**A**) Low expression of RIP1 (red) in WT retina at P120. Cones identified by PNA staining (green); nuclei counterstained with DAPI. ONL, outer nuclear layer; INL, inner nuclear layer. (**B**) RIP1 (red) labels all rod and cone photoreceptors in P23H retina. RIP1 localization in cone photoreceptors confirmed with PNA/RIP1 co-labeling (yellow) inset: higher magnification of co-localization. Arrow, nuclear fragmentation. (**C**) No RIP3 (green) labeling in WT retina. Rod photoreceptor outer segments labeled with rhodopsin (RHO, red) antibody. Scale bar in (A–C) = 20 µm. (**D**) Co-localization of RIP3 (green) with rod photoreceptor cells (red) in P23H retina at P120. Inset: higher magnification of co-localization at the base of the rod outer segment (OS). (**E**) RIP3 expression (red) does not co-localize with PNA labeling of cone cells (green). (**F**) Co-localization of RIP3 (green) with rod photoreceptor cells (red) in P23H retina at P21. Scale bar in (D–F) = 10 µm. Representative confocal images in (A–F) are from eyes of each of six animals per age group ($n = 12$) from two independent experiments. Immunoblots of temporal protein expression levels for RIP1 protein (**G**), RIP3 protein (**H**) and (**I**) two LC3 isoforms from retinal extracts P21, P45 and P120. LC3 expression only shown at P120. Protein loading control, β-actin. Blots are representative of three independent experiments. (**J**) Comparison of LDH activity in WT and P23H vitreous sample at P120. Data plotted as mean ± SEM ($n = 3$), and statistical significance was determined using the Student *t*-test, $^*P < 0.01$.

marker expression in activated microglia and this co-localized with the presence NLRP3 in about one-third of the cells (Fig. 5G), indicating inflammasome activation in retinal microglia. A 25-fold increase in the number of Iba-1-positive cells in P23H-1 retina was also observed, indicative of large microglia infiltration (Fig. 5I).

Since inflammasome activation has been detected in damaged retinal pigment epithelium (RPE) cells in age-related macular degeneration (AMD) (32) we also looked for the presence of NLRP3 and cleaved caspase-1 in the RPE of P23H-1 eyes. By WB analysis no up-regulation of these markers was observed in RPE extracts from either WT or P23H-1 animals up to P120 (Supplementary Material, Fig. S1A). Furthermore, there was no loss of tight junction integrity between P23H-1 RPE cells (Supplementary Material, Fig. S1B and C) that has been described in RPE undergoing inflammasome activation associated with the release of IL-18 (32). This suggests that pro-inflammatory cytokines are not released from the RPE to cause photoreceptor damage in the P23H-1 model. We did note, however, that at 1 year of age the RPE had started to lose its tight junction integrity (Supplementary Material, Fig. S1D), which could be in response to secretion of IL-18 from the P23H retina causing RPE cell death.

Effect of cell-death inhibitors in the P23H-1 retina

To further validate the role of the various cell-death pathways activated in the P23H-1 model, we looked at the effects of known inhibitors including: calpeptin (a calpain inhibitor); 3-aminobenzamide (3-AB, a PARP inhibitor); necrostatin-1s (Nec-1s, a RIP1 inhibitor) and *N*-acetylcysteine (NAC anti-oxidant/inhibitor of NLRP3). Rats received once daily subcutaneous injections of drugs that started at P21 and continued until P120. Histological analysis of retinal sections taken from central retina locations (superior and inferior loci in the posterior pole of the eye), in P120 WT, sham-treated and drug-treated mutant retina were examined. The ONL thickness in sham-treated animals was only 2–4 nuclei, whereas WT retina had an ONL thickness of 10–12 nuclei at P120 (Supplementary Material, Fig. S2). All test compounds resulted in some preservation of ONL thickness (four to six nuclei thick), except 3-AB, which appeared to have little effect. A more rigorous, spiderplot comparison was made to quantitatively compare the ONL thickness for the entire retina (Fig. 6A). This revealed that across the retina overall, most histological benefit was obtained with Nec-1s, followed by NAC, calpeptin and 3-AB treatments (Fig. 6B).

We also examined the effect of the different cell-death inhibitors on rod photoreceptor function by measuring maximum *b*-wave amplitudes generated by electroretinography (ERG) after dark adaptation *in vivo*. In the sham-treated P23H-1 rats at P21 the *b*-wave amplitude was already reduced from WT levels by 30% (450 µV versus normal maximum *b*-wave amplitude is ~625 µV), followed by a gradual decline over time to 225 µV at P120. All cell-death inhibitors to some extent slowed the decline in retinal ERG responses to ~300 µV at P120 (Fig. 6C). Statistical

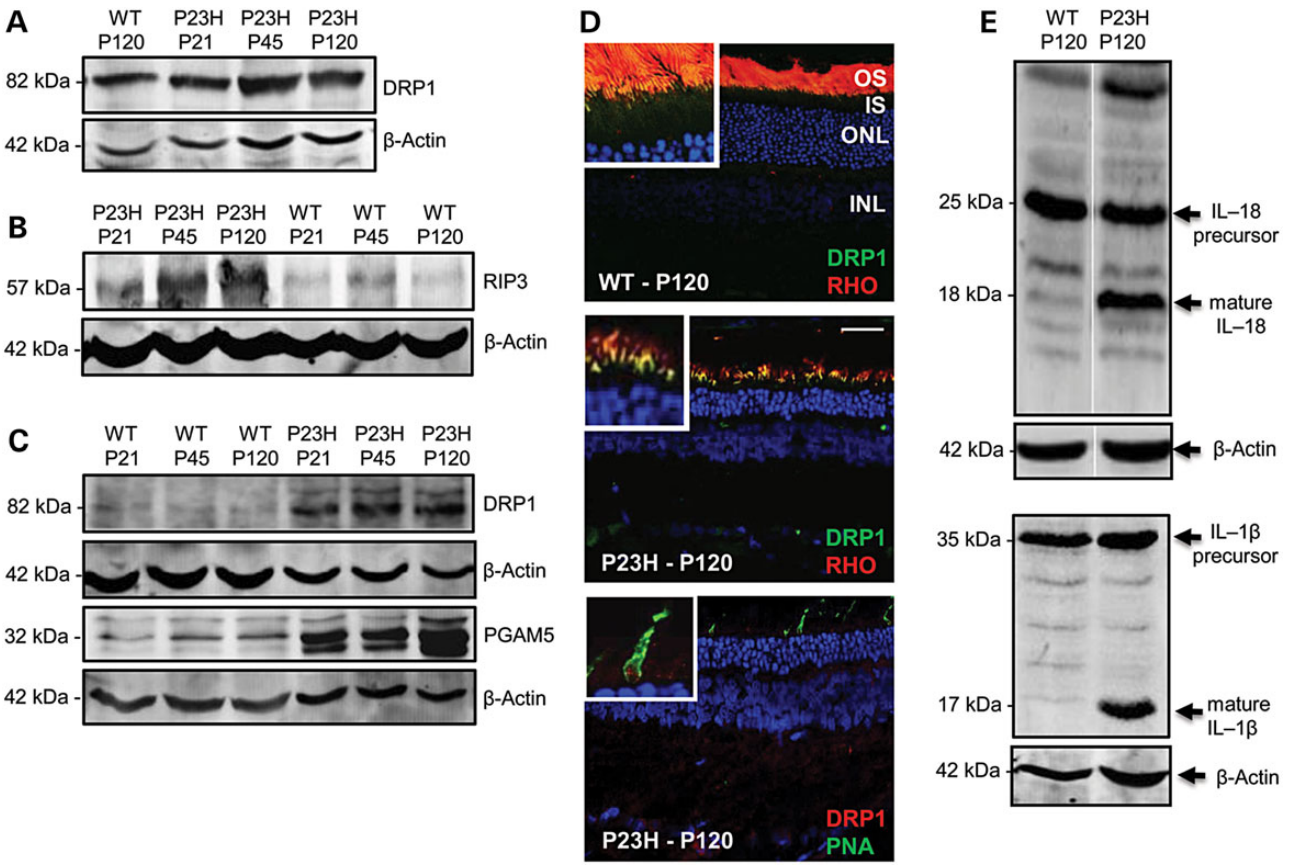

Figure 3. Expression of downstream targets of RIP3. (**A**) Immunoblots from two independent experiments show DRP1 expression levels in WT and P23H mutant retinal extracts from six eyes each at P21, P45 and P120. (**B**) Immunoblots of the RIP3 expression levels in WT and P23H mutant mitochondrial fractions from retinal extracts at P21, P45 and P120. (**C**) Immunoblots showing temporal expression of the DRP1 and PGAM5 proteins in the mitochondrial fraction of retinal extracts in from WT and P23H eyes. (**D**) Merged images of DRP1 (green) and rhodopsin (red) co-localization in mitochondria at the inner segment (IS)/outer segment (OS) boundary (inset) of P23H rod photoreceptors, compared with low levels of DRP1 in WT photoreceptor IS/OS (inset). Lower panel, low-DRP1 expression (red) in cone photoreceptors (green PNA labeling). Size bar = 20 μm. The eyes of each of three animals per age group ($n = 6$) from two independent experiments were examined. (**E**) The presence of both mature IL-18 and IL-1β in P23H mutant whole eye extracts indicative of active inflammatory protein processing events. Loading control, β-actin.

significance was determined using two-way analysis of variance (ANOVA) on the five different P23H-1 treatment groups. This showed significant effects of time ($P = 0.025$) and treatment ($P = 0.008$). *Post hoc* (Tukey) comparisons between treatment groups showed significant effects of calpeptin versus sham ($P < 0.03$); 3AB versus sham ($P < 0.01$); Nec-1s versus sham ($P < 0.01$) and NAC versus sham ($P < 0.01$).

Photoreceptor outer segments were assessed with a rhodopsin antibody to determine whether cell-death inhibitor treatment had any effect on inner segment/outer segment integrity. Nec-1s, NAC and calpeptin appeared to result in elongated outer segments and improvements to the photoreceptor structural organization compared with sham-treated retina or treatment with 3-AB (Fig. 6D). WB assessment demonstrated little PARP expression in either 3-AB-treated or sham-treated P23H-1 retina (Fig. 6E). Nec-1s eliminated RIP1 expression (Fig. 6F), decreased RIP3 expression by 4-fold (Fig. 6G) and also reduced the expression of NLRP3 (Fig. 6H). NAC treatment resulted in a 50% decrease in NLRP3 expression (Fig. 6I).

We also examined the effect of the cell-death inhibitors specifically on cone photoreceptor survival (P45–P120). In the P23H-1 model, cone-cell survival is compromised after the peak of rod cell death has occurred (33). Calpeptin and 3-AB had no effect on preventing cone loss or preserving cone morphology compared with sham-treated controls (Fig. 7A–C), whereas rats treated with Nec-1s or NAC had elongated cone outer segments (Fig. 7D and E). This preservation in morphology was quantified by counting PNA-positive cone photoreceptors in retinal flat-mounts (Fig. 7F–H) as previously described (34). This highlighted a significant increase in the number of cones in treated eyes compared with sham-treated controls (Fig. 7I; $P < 0.01$, $n = 6$). We have shown that RIP1 (Fig. 2B) and NLRP3 (Fig. 4F) are expressed in degenerating cones. Inhibition of RIP1 by Nec-1s and inhibition of NLRP3 expression by NAC might explain the survival of these cones. We examined the expression of phosphorylated NF-κB since ubiquitylation of RIP1 promotes activation of NF-κB-mediated pro-inflammatory pathway and suppresses the activation of the RIP1 kinase activity required for RIP3-dependent necroptosis (35). We found that at P120, P23H-1 mutant retinal extracts had a high level of expression of NF-κB compared with WT controls, and that treatment with Nec-1s reduced NF-κB expression by 15-fold (Fig. 7J). One of the downstream effects of RIP1 activity is NF-κB-mediated IL-1α secretion (36). Quantitative RT-polymerase chain reaction (PCR) revealed that in P23H-1 retina there was a 5-fold increase in IL-1α expression, whereas treatment with Nec-1s significantly reduced IL-1α expression to only 1-fold (Fig. 7K; $P < 0.01$, $n = 5$), suggesting that up-regulation of IL-1α was a RIP1-dependent response in the P23H-1 retina.

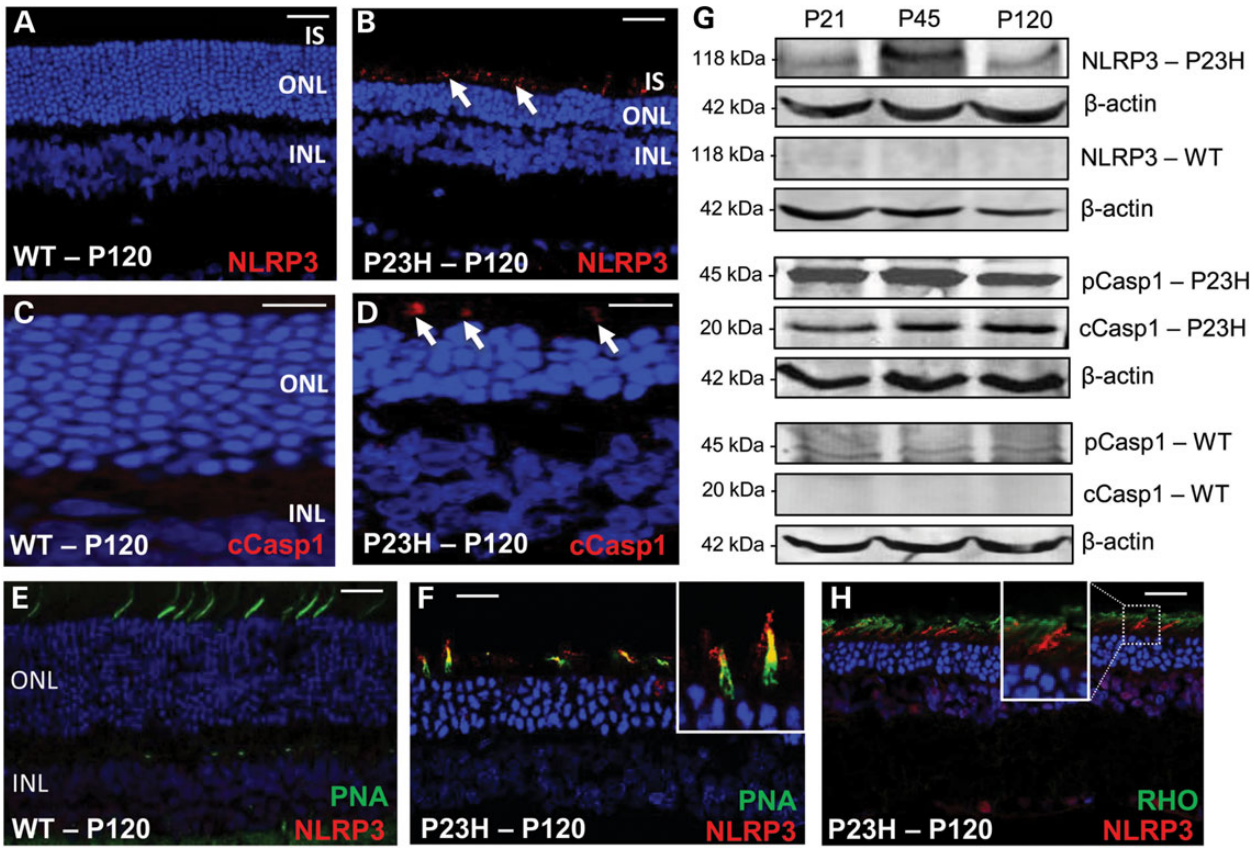

Figure 4. Expression of markers of inflammasome activation in WT and P23H rat retina. Representative confocal images are from eyes of each of three animals per age group ($n = 6$) from two independent experiments. (**A** and **B**) Arrows point to localization of NLRP3 (green). IS, inner segments; ONL, outer nuclear layer; scale bar = 5 µm. (**C** and **D**) Arrows point to localization of cleaved caspase-1 (cCasp1) in red. INL, inner nuclear layer. Scale bar = 10 µm. (**E** and **F**) co-labeling of NLRP3 (red) with PNA labeling of cone photoreceptors (green) in WT or P23H retina. Scale bar = 20 µm. (F) Inset shows co-localization of NLRP3 at higher magnification in a cone photoreceptor. (**G**) Immunoblots of NLRP3, pCasp1 and cleaved caspase-1 (cCasp1) expression in WT and P23H retinal extracts from six eyes at P21, P45 and P120. Blots are representative of two independent experiments. (**H**) NLRP3 (green) does not co-localize with mutant rod photoreceptors (red).

The cone function was measured by the 30 Hz flicker ERG response *in vivo* and treatment with Nec-1s resulted in a 30 Hz flicker response that was not significantly different from WT at P120 ($P < 0.20$, $n = 10$), whereas the other cell-death inhibitors all resulted in a smaller 30 Hz flicker ($P < 0.01$, $n = 10$), but better than sham-treated controls (Fig. 7L). Statistical significance was determined using two-way ANOVA on the P23H-1 treatment groups, and showed significant effects of time ($P = 0.018$) and treatment ($P = 0.008$). *Post hoc* (Tukey) comparisons between treatment groups showed significant effects of calpeptin versus sham ($P < 0.001$); 3-AB versus sham ($P < 0.01$) and NAC versus sham ($P < 0.03$). The data from these cell-death inhibitor studies support the concept that cone cell death is dependent on both inflammasome activation as well as a RIP1-mediated inflammatory response.

Quantitative analysis of TUNEL-positive cells in the retina after treatment with individual cell-death inhibitors revealed significantly fewer TUNEL-positive cells than in untreated eyes for calpeptin, Nec-1s and NAC at P45 (Fig. 8A), but at P120 only Nec-1s resulted in significantly fewer TUNEL-positive cells ($P < 0.05$, $n = 8$). At neither timepoint did 3-AB have any effect on cell death (Fig. 8A). Since DRP1 activity promotes mitochondrial damage (fission) and the subsequent production of reactive oxygen species, we examined carbonyl adduct formation derived from protein oxidation (37). In P23H-1 retina, the carbonyl content was significantly increased at P120 ($P < 0.05$, $n = 6$), whereas treatment with Nec-1s and NAC lowered the carbonyl content, reflecting less oxidative damage to the retina (Fig. 8B). Furthermore, since we previously observed mature IL-1β expression in P23H-1 retina we also examined whether NAC affected cytokine expression (NAC inhibits NLRP3 and inflammasome activation) (38). At P120, the amount of IL-1β was significantly reduced by 90% ($P < 0.001$, $n = 6$) (Fig. 8C). Since NLRP3 inflammasome activation requires a priming step, mostly via a cell-surface receptor we examined whether P2RX7, a well-known inflammasome activator (39,40), was the cause of up-regulated NLRP3 in cone photoreceptors. One eye of P23H-1 animals at P120 was treated with an intravitreal injection of the P2RX7 inhibitor Brilliant Blue G (BBG) (41), whereas the other eye was injected with vehicle control. Retinas were analyzed 1 week later by WB. This revealed a down-regulation of NLRP3, cleaved caspase 1 and mature IL-1β proteins in the treated eyes (Fig. 8D). These results suggest that cones are responding to extracellular levels of adenosine triphosphate (ATP) (42) that can trigger activation of the inflammasome via the P2RX7 receptor. Dying and dead cells release a wide array of molecules including ATP and high-mobility group box-1 protein (HMGB1) (43). We investigated the gene expression levels of *HMGB1*, as well as *IL-18* and *IL-1β* and found that these genes were all up-regulated in P23H-1 retinas (Fig. 8E).

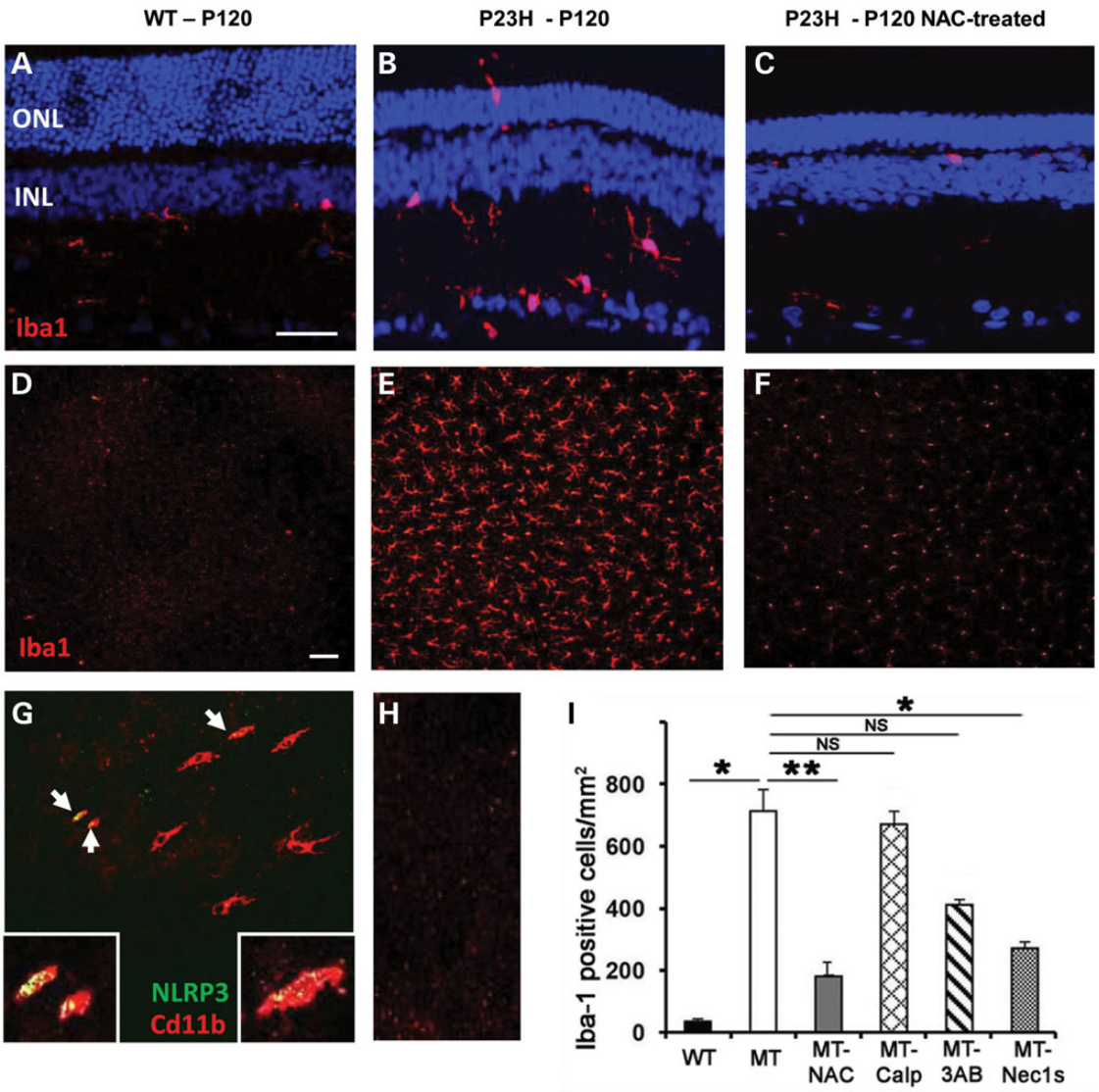

Figure 5. Microglial activation in WT and P23H rat retina at P120. (**A–C**) Sagittal sections through retina showing localization of Iba1 (red) that labels resting and activated microglial cells. ONL, outer nuclear layer, INL, inner nuclear layer. Size bar in (A–C) = 50 µm. P23H retina treated with N-acetylcysteine (NAC). (**D–F**) Images of retinal whole-mount (photoreceptor surface facing up) showing Iba1-positive cells across the retina in P23H retina. Scale bar in (D–F) = 100 µm. Representative images in (A–F) are from eyes of each of three animals per age group ($n = 6$) from two independent experiments. (**G**) About one-third of retinal microglial cells co-expressed inflammasome marker NLRP3 (green) and the activated microglial surface marker Cd11a (red). (**H**) Negative control for (G) (no primary antibodies). (**I**) Quantification of the number of Iba-1 positive cells with different treatments in P23H mutant (MT) retina. NAC, N-acetylecysteine; Calp, calpeptin; 3AB, 3-aminobenzamide; Nec1s, necrostatin-1s. Data presented as mean ± SEM ($n = 6$ per treatment). Statistical significance was determined using the Student *t*-test; $^{*}P < 0.01$; $^{**}P < 0.001$. NS, not significant.

Finally, since we saw a 25-fold increase in the number of microglia in the mutant retina (Fig. 5I) we investigated the effect of the different inhibitors on microglial activation. Immunocytochemistry revealed fewer microglia in the NAC-treated retina compared with untreated controls (Fig. 5C and F) and quantification showed that both NAC and Nec-1s reduced significantly the number of microglia present in the retina ($^{*}P < 0.001$, $n = 6$), compared with the other inhibitors (Fig. 5I).

Cone cell death in the P23H mouse is an *Nlrp3*-dependent process

Since our data revealed that components of the NLRP3 inflammasome were activated during cone photoreceptor cell death, we generated a mouse line that expressed the heterozygous P23H rhodopsin mutation (44) on an *Nlrp3*$^{-/-}$ knock-out background (45) to see if we could prevent cone cell death. By western blotting NLRP3 was not detectable in WT or *Nlrp3*-deficient retinal or RPE extracts (Fig. 9A). In contrast NLRP3 was up-regulated in the P23H retina, however, it was not detectable in P23H;*Nlrp3*$^{-/-}$ retina nor in RPE extracts, demonstrating that genetic deficiency of *Nlrp3* was confirmed at the protein level in the retina. Since NLRP3 interacts with pro-caspase 1 leading to its cleavage, we also tested for cleaved Casp1 (cCasp1). Low levels of cCasp1 were present in WT and *Nlrp3*$^{-/-}$ retinal and RPE extracts; however, in P23H retina we observed a 10-fold increase in cCasp1 expression (Fig. 9A). On the P23H;*Nlrp3*$^{-/-}$ background expression of cCasp1 was reduced to background. The downstream target of inflammasome activation is processing of the precursor form of IL-1β to its mature form by cCasp1. The mature IL-1β was detected in P23H retinal

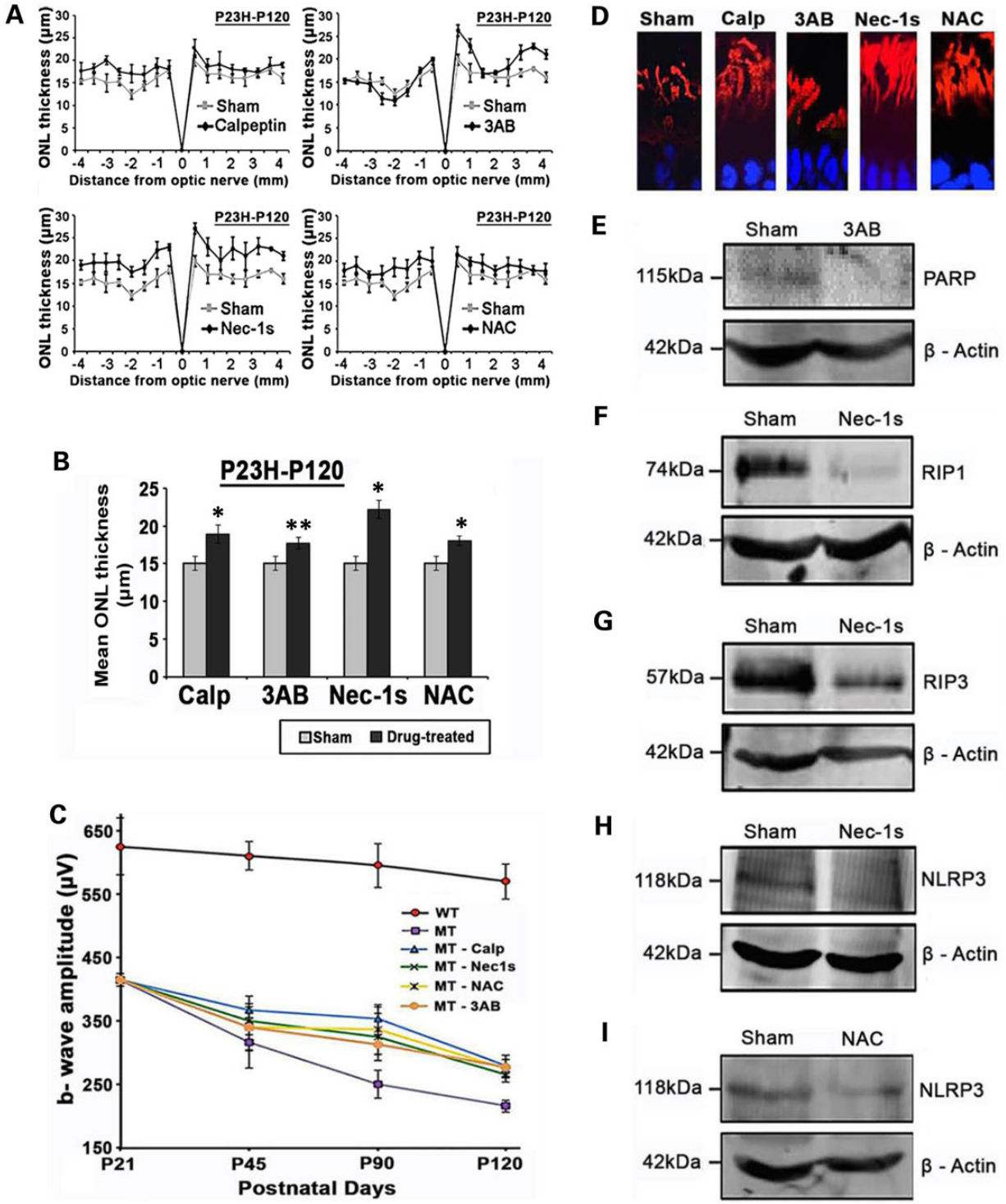

Figure 6. The effect of inhibitory compounds on the retina. (**A**) Spider plot of ONL thickness in the retina in sham and drug-treated P23H rats at P120. (**B**) The mean ONL thickness across the whole retina was analyzed by averaging the measurements used in spider plots. Data presented as mean ± SEM, ($n = 6$ eyes per group). Statistical significance was determined using Student's *t*-test,*$P < 0.001$; **$P < 0.01$. (**C**) Comparison of maximum dark-adapted ERG *b*-wave responses analyzed at P21, P45, P90 and P120 for WT and drug-treated retinas. Data plotted as mean ± SEM ($n = 12$ eyes per group). (**D**) Rhodopsin labeling (red) of sham or drug-treated photoreceptor outer segments. Calp: calpeptin; 3AB, 3-aminobenzamide; Nec1s, necrostatin-1s, NAC, *N*-acetylcysteine. (**E**) Immunoblot of PARP in retinal extracts from P23H retina with sham or 3-AB treatment. Loading control β-actin. (**F**) Immunoblot of RIP1 in retinal extracts from P23H retina with sham or Nec-1s treatment. (**G**) Immunoblot of RIP3 retinal extracts from P23H retina with sham or Nec-1s treatment. (**H**) Immunoblot of NLRP3 retinal extracts from P23H retina with sham or Nec-1s treatment. (**I**) Immunoblot of NLRP3 retinal extracts from P23H retina with sham or NAC treatment. All immunoblots were tested on retinal extracts from three eyes per treatment group.

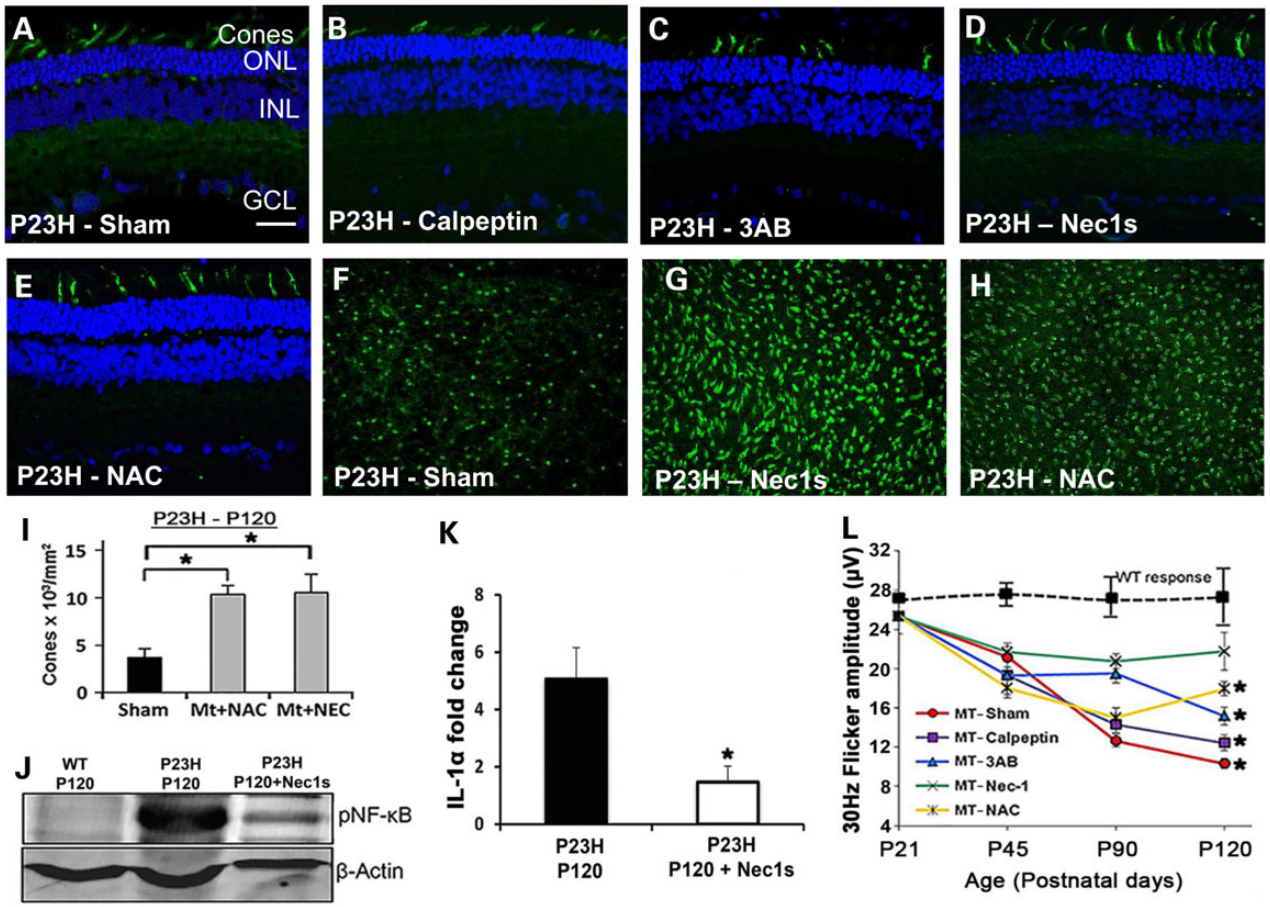

Figure 7. The effect of inhibitory compounds on cone photoreceptor viability. Representative sagittal sections ($n = 12$) through P23H central retina at P120 that were (**A**) sham-treated; (**B**) treated with calpeptin; (**C**) 3-AB, 3-aminobenzamine; (**D**) Nec1s, necrostatin-1s; (**E**) NAC, *N*-acetylcysteine. Cones are labeled with PNA (green) and nuclei stained with DAPI. ONL, outer nuclear layer; INL, inner nuclear layer; GCL, ganglion cell layer. Scale bar in (A) = 20 μm and is the same in all panels. PNA-labeling of cones in retinal flatmounts at P120 that were (**F**) sham-treated, (**G**) treated with Nec1s or (**H**) treated with NAC. (**I**) Quantification of PNA-labeled cones in (F–H). Statistical significance was determined using ANOVA. * $P < 0.01$, ($n = 6$ eyes per group) (**J**) Expression of phosphorylated NF-κB in WT retina compared with P23H retina in the presence or absence of Nec1s at P120. β-actin used as loading control. (**K**) Semi-quantitative PCR of IL-1α expression in mutant and Nec1s-treated P120 P23H retina. Nec1s resulted in a 4 fold reduction in IL-1α expression (*$P < 0.05$, $n = 6$). (**L**) 30 Hz Flicker responses from the electroretinogram, representing cone function over length of treatment time. *$P < 0.05$. Data plotted as mean ± SEM ($n = 10$ per treatment).

samples, but not in retina from P23H;*Nlrp3*$^{-/-}$ mice (Fig. 9A). In the P23H;*Nlrp3*-deficient retina there were significantly more cones than in P23H retina, both qualitatively as observed by IHC (Fig. 9B) and quantitatively (Fig. 9C; 19×10^3 versus 12×10^3 cones/mm^2, respectively; $n = 5$, $P < 0.01$). The *in vivo* 30 Hz flicker response in cones from the P23H;*Nlrp3*$^{-/-}$ retina was significantly better than P23H retinal responses ($n = 5$, $P < 0.05$), and was within the normal range of WT responses (Fig. 9C). Together these data demonstrate that cone cell death in the P23H mouse mutant is an inflammasome-dependent process.

Discussion

Through anatomical, genetic and functional studies in the P23H rhodopsin model of retinal degeneration we have identified several different cell-death pathways that are active and identify a new pathway for bystander cone cell death. In rod photoreceptors, cell death occurs principally through necroptotic-mediated signaling whereas activation of the NLRP3 inflammasome occurs in cone photoreceptors and retinal macrophages (Supplementary Material, Fig. S3). Our data, therefore, highlight that distinct, photoreceptor-specific mechanisms drive P23H retinal degeneration and suggests that limiting both the inflammasome-driven response and necrotic signaling is pivotal in designing therapeutic strategies to prevent cell loss.

Previous studies of later photoreceptor cell-death signaling in the P23H model have implicated caspase-independent apoptosis (8) and autophagy (23). Other work has also highlighted oxidative stress and the production of ROS (46). In our current study, we find that caspase-independent cell death seems to be a pan-retinal response, but might only be a minor player in photoreceptor cell death. This is because few cells express the relevant markers and the relevant inhibitors (calpeptin and 3-AB) have a smaller effect on numbers of TUNEL-positive cells in comparison with the effects of inhibiting necroptosis (Nec-1s). Furthermore, our finding that there is a little change in LC3 processing suggests that autophagy is also a lesser consideration. This contrasts with previous studies (23) probably because animals were only studied animals up to P60 whereas in our study LC3 was assessed at much later timepoints.

Most cell-death studies in the P23H model have concentrated on earlier signaling events. For example, studies have demonstrated that misfolded and abnormally glycosylated P23H rhodopsin is retained and degraded within the ER (6,7,47–49)

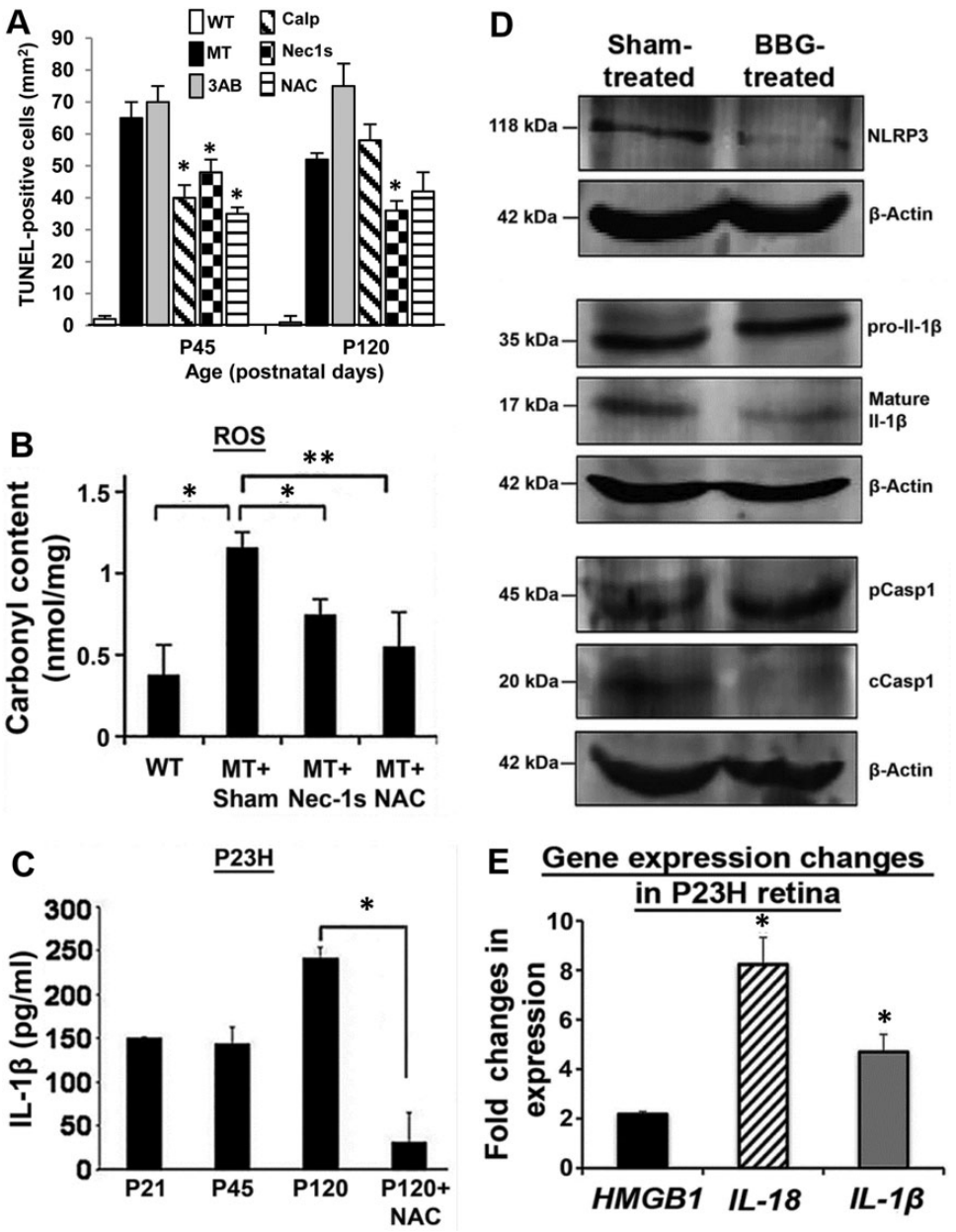

Figure 8. Quantitation of inflammasome activation and inhibition of the P2RX7 receptor. (**A**) TUNEL-positive cell counts at P45 and P120 in WT, P23H (MT), MT + Calp, MT + 3AB, MT + Nec1s and MT + NAC. Data plotted as mean ± SEM ($n = 8$ per treatment); *$P < 0.05$. (**B**) Carbonyl content in retinal extracts of WT and MT retina treated with Nec-1s and NAC at P120. Data from two independent experiments in triplicate, plotted as mean ± SEM. *$P < 0.05$ and **$P < 0.01$. (**C**) Quantification of IL-1β protein in P23H retinal extracts at P21, P45 and P120 with or without NAC treatment. Data plotted from two independent experiments in triplicate, as mean ± SEM. *$P < 0.001$. (**D**) Immunoblots of NLRP3, pro-IL-1β, mature IL-1β, pCasp1 and cCasp1 in P23H rat retinal extracts ($n = 6$) that was either sham-treated or treated with BBG. β-actin was used as a loading control. (**E**) Semi-quantitative RT-PCR to measure the change in gene expression levels of *HMGB1*, *IL-18* and *IL-1β* compared with untreated P23H eyes. Data from two independent experiments in triplicate ($n = 6$), plotted as mean ± SEM. *$P < 0.05$. Statistical significance was determined using Student's *t*-test.

promoting ER stress pathways (50). Reducing stability and ER exit of P23H rhodopsin by preventing chromophore binding can promote cell death (51) and retinal degeneration (52,53), and that measures directed at ER stress reduction can alleviate retinal degeneration (54). We hypothesize that the established ER-stress response in the P23H-1 model results either directly or indirectly in necroptosis in rod photoreceptors due to up-regulation of RIP3/RIP3 complexes and DRP1/PGAM5 activity, that subsequently leads to an influx of calcium into mitochondria (55) that precipitates necroptosis (27). A major role for necroptosis is also implied by our results showing elevated LDH, a hallmark feature of necrotic tissue (25). Although necroptosis has also been implicated in the pathophysiology of other retinal diseases such as AMD (56), retinal detachment (57) and retinal ischemia (58), it has not been reported in adRP.

Secondary death of cones in RP has been the topic for much recent work and has led to many hypotheses as to why such 'bystander' cell death occurs (20). Proposed pathways include: oxidative stress and ROS production (59); reduced secretion of rod-derived cone viability factor (60); nutritional deficits inhibiting the insulin/mTOR pathway (61) and nitric oxide release from glia cell activation (62). Our results alternatively highlight

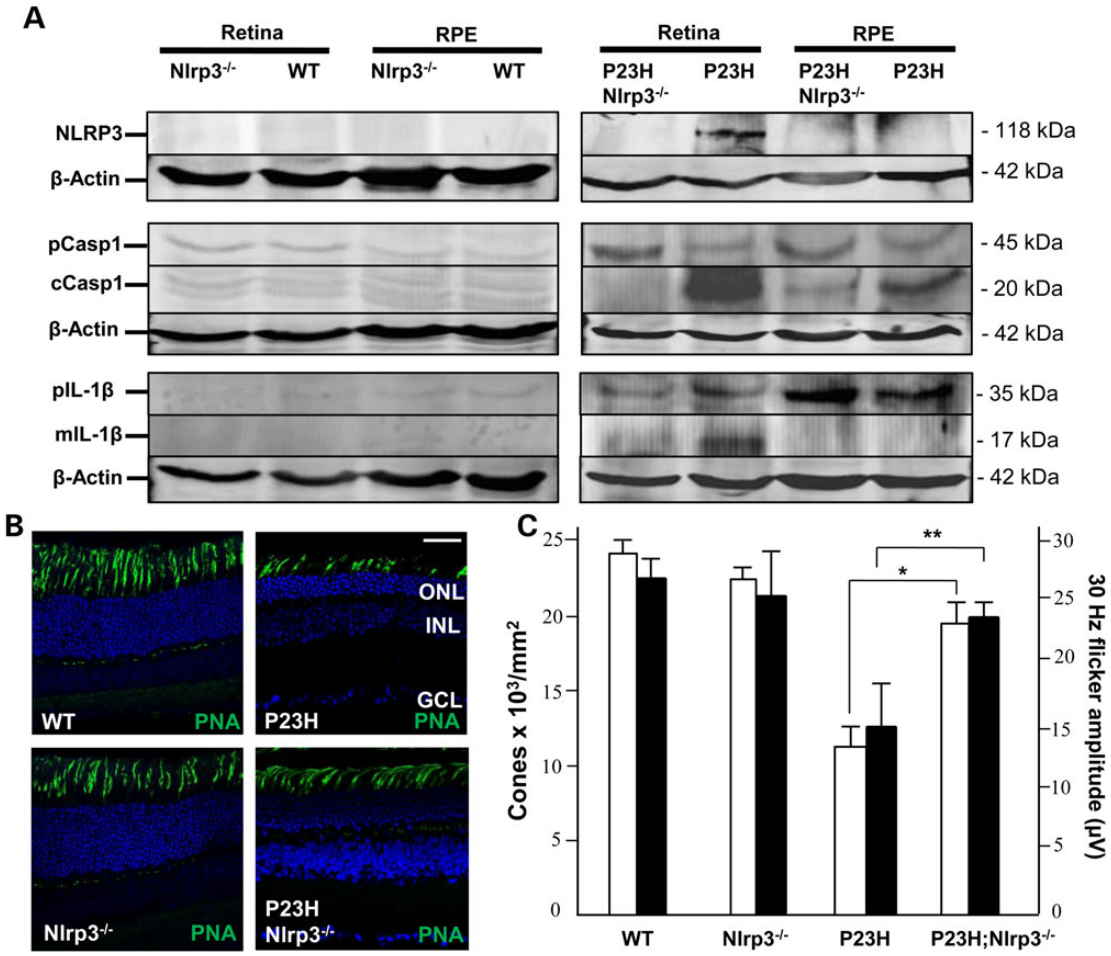

Figure 9. Inflammasome activation and cone cell death in different P23H genotypes. (**A**) Western blots in retinal and RPE extracts from each genotype for NLRP3, pCasp1, cCasp1, Pro-IL-1β (pIL-1β) and mature IL-1β (mIL-1β). β-actin was used as the loading control. (**B**) Representative sagittal sections through the central retina of mice at P120 ($n = 6$). Cones are labeled with PNA (green) and nuclei stained with DAPI. ONL, outer nuclear layer; INL, inner nuclear layer; GCL, ganglion cell layer. Scale bar in P23H image = 20 μm and is the same in all panels. (**C**) Dual histogram showing the quantification of the number of cones for each genotype (left axis, white bars) and 30 Hz Flicker responses from the electroretinogram (right axis, black bars). Data plotted as mean ± SEM ($n = 5$; $^{*}P < 0.01$ and $^{**}P < 0.05$).

a central role for inflammasome activation and pyroptosis in this bystander effect. Our data on the P23H mutation on the *Nlrp3*-deficient background confirm that secondary cone cell death is an inflammasome-dependent process. This is supported by our results, which show that the P2RX7 antagonist BBG inhibits the up-regulation of inflammasome components in cones. We hypothesize that activation of P2RX7 receptors leads to assembly of the NLRP3 inflammasome either directly (63) or via ROS (64), with subsequent increased IL-1β and IL-18 cytokine production and ensuing pyroptosis. P2RX7 receptors respond to local extracellular ATP levels (42) and it has already been shown that P23H retina tissue has elevated levels of ATP (26). We propose that rod photoreceptors undergoing necroptotic cell death, release their cellular contents including bioactive molecules such as ATP and the 'damage-associated molecular pattern molecule' HMGB1, which leads to inflammasome activation in cones. Thus, inhibition of the RIP1/RIP3 pathway in rods to prevent HGMB1 release may also be a potential target to dampen secondary cone cell loss. Together these results suggest that secondary cone cell death occurs via pro-inflammatory mechanisms.

Other disease models have demonstrated dysregulation of the inflammasome in chronic disease, for instance, in: gout; atherosclerosis; Alzheimers and type 2 diabetes (65). In eye disease, activation of the inflammasome has only been reported in AMD in the RPE layer of the retina (32). There is, however, growing clinical evidence to suggest that there is an inflammatory component in human RP (66). Furthermore, induced recruitment of microglia to the retina (67) and retinal preservation using anti-oxidant/anti-inflammatory drugs (68) have also been shown in retinal degeneration models. Recently, it has been suggested that the anti-inflammatory effect of NAC occurs via inhibition of mRNA expression of NLRP3, Il-18 and IL-1β (38). Our data provide direct evidence that treatment with NAC not only inhibited NLRP3 and Il-1β expression thereby preserving cone viability, but also reduced the number of retinal microglia.

Our findings are in contrast to recent work in the *rd10* mouse (34). In that study, *rd10* mice were crossed with *Rip3* knock-out mice to generate *rd10*/*Rip3*$^{-/-}$ animals that were subsequently treated with Nec-1 and pan-caspase inhibitor IDN-6556. That study concluded that cone photoreceptors in this model die via necroptosis and rods probably by apoptosis. This difference in late cell-death signaling between the *rd10* and P23H mice is possibly explained by the fact that the genetic abnormalities in these two models are very different; the former resulting in a loss-of-function phenotype whereas the later results in a gain-of-function ER-stress response. It is likely that different

cell-death pathways are triggered in different RP genotypes. This would also explain for instance why necroptosis has been implicated in both rod and cone cell death in the interphotoreceptor retinoid-binding protein-deficient mouse model of RP (69). Previous published data on the P23H model may also warrant re-interpretation. For example, it has been suggested that XIAP gene therapy in the P23H rat preserves retinal structure and ERG responses by inhibition of caspase-3, -7 and -9 (70). However, no evidence was provided in the study to demonstrate that the activity of these three caspases was reduced. Our results show limited presence of activated caspase-3 in the degenerating P23H retina, which is in agreement with other studies that show caspase-3 and -9 do not significantly contribute to the underlying pathology in the P23H model (21). Alternatively, it has been shown that XIAP also inhibits RIP3-dependent cell death and activation of the inflammasome in dendritic cells (19), thus we propose that it is this mechanism at play when XIAP gene therapy rescues the P23H animal rather than inhibiting apoptosis.

One significant consequence of identifying the cell-death signaling response in RP is the opportunity for therapeutic benefit. This has led to a number of pre-clinical studies seeking to enhance or inhibit the unfolded protein response (UPR) (50,71–73); however, these studies have not fully clarified the role of the UPR in rhodopsin-mediated cell death. Other studies have attempted to prevent cell death directly (8). It is particularly notable, however, that inhibition of individual pathways in isolation never seems to completely stop degeneration and also this limited histological benefit is often associated with even less functional benefit (74). One possible explanation for this disconnect between histological and functional benefits may be that in any particular degeneration, as seen in this study, many cell-death signaling pathways are triggered such that individually targeting any single pathway is unlikely to have a large effect. This could suggest that a combination drug strategy where a number of drugs target multiple pathways might be more effective.

In summary, these studies reveal NLRP3-dependent inflammasome activation as a new molecular mechanism driving cone photoreceptor cell death in one of the most common forms of human RP. Such cell death, via bystander cell signaling, has been shown to be an important phenomena in many other systems, for instance: during development in (75); infection (76); neurological disease (77) and Alzheimer's disease (78). The phenomenon of bystander cell death has also been used therapeutically to treat cancer (79). Activation of the inflammasome may explain why previous therapeutic strategies targeting P23H mutant protein do not fully rescue the progression of disease in the long term, and suggests that combination therapy targeting the inflammasome in addition to other identified cell-death pathways might be more beneficial.

Materials and Methods

Animals

Homozygous P23H-1 transgenic rats (obtained from Professor Matt LaVail, University of California at San Francisco, CA, USA) were crossed to WT pigmented Long–Evans rats to obtain heterozygous offspring for these studies. Homozygous P23H knock-in mice and *Nlrp3* knock-out mice were obtained from Jackson Labs and crossed to generate double heterozygote offspring and then backcrossed to generate P23H;*Nlrp3*$^{-/-}$ mice. Animals were maintained on a 12 h light/dark cycle and research carried out in accordance with protocols compliant to the Canadian Council on Animal Care with the approval of the Animal Care Committee at the University of British Columbia and with the Association for Research in Vison and Ophthalmology statement for the use of animals in vision research. Equal numbers of male and female rats and mice were used in this study. Rats received once daily subcutaneous injection of various cell-death inhibitors: RIP1 inhibitor, necrostatin-1s (Biovision), 15 mg/kg body weight; PARP inhibitor, 3-aminobenzamide (Sigma-Aldrich), 25 mg/kg body weight; calpain inhibitor, calpeptin (Calbiochem), 250 μg/kg body weight; anti-oxidant, NAC (Sigma-Aldrich), 150 mg/kg body weight. For sham treatments rats received daily phosphate buffered saline (PBS) injections. Treatment started at P21 and continued until P120.

Antibodies

Primary antibodies [catalog number, dilution and application WB; IHC) were obtained from Sigma-Aldrich: β-actin (A5441, 1:3000 WB), RIPK1 (SAB3500420, 1:200 IHC, 1:500 WB), RIP3 (PRS2283, 1:1000 WB); from Abgent: RIPK3 (AP7184a, 1:1000 IHC, 1:500 WB), from Cell Signalling: cleaved caspase-3 (9661s, 1:200 IHC), DRP1 (8570, 1:200 IHC, 1:1000 WB), from Abcam: LC3 (ab48394, 1:500 WB), IL-1β (ab9722, 1:200, IHC, 1:500 WB), PARP (ab110915, 1:200 IHC, 1:1000 WB); NLRP3 (ab91413, 1:200 IHC, 1:500 WB), Cd11b (ab8879, 1:200 IHC), rhodopsin 1D4 (ab5417, 1:500 IHC); from Santa Cruz: IL-18 (7954, 1:200 WB), NF-κB (sc-101749, 1:250 WB); from Millipore: caspase-1 (AB1871, 1:50 IHC, 1:500 WB), from Wako: Iba1 (019-19741, 1:300 IHC); from Invitrogen: ZO-1 (40-2200, 1:100 IHC). Secondary antibodies [catalog number, dilution and application (WB; IHC)] were obtained from Invitrogen: AlexaFluor® 594 goat anti-mouse IgG (A-11005, 1:200 IHC), AlexaFluor® 488 goat anti-mouse IgG (A-11001, 1:200 IHC), AlexaFluor® 488 goat anti-rabbit IgG (A-11008, 1:200 IHC), AlexaFluor® 594 goat anti-rabbit IgG (A-11012, 1:200 IHC); from Rockland: Rabbit antibody IR Dye800 conjugated (611-132-003, 1:15 000 WB). Fluorescently conjugated lectins were as follows: fluorescein isothiocyanate-PNA (Sigma-Aldrich, L7381, 1:100, IHC), AlexaFluor® 568 phalloidin (A12380, 1:100, IHC).

Histology and IHC

Eyes were fixed in 2.5% glutaraldehyde in 0.1 M sodium cacodylate buffer fixative (Electronmicroscopy Sciences) for 1 h prior to processing. For histology paraffin-embedded eye sections (4–6 μm thick) were stained with hematoxylin and eosin (H&E and photographed using an Olympus BX46 Clinical Microscope in the superior or inferior central retina. For cryostat sectioning, eyes were cryopreserved in 30% sucrose overnight, snap frozen and then embedded in Polyfreeze medium (Polysciences). Sagittal sections (~10 μm thick) were incubated overnight at 4°C with primary antibody diluted in blocking buffer (2% normal goat serum, 0.1% Triton X-100 in PBS). After extensive washes in PBS-Tween 20, localization of antibody labeling was detected after a 1 h incubation with secondary antibody diluted in PBS containing 2% normal goat serum. Nuclei were counter stained with 4′, 6-diamidino-2-phenylindole (DAPI). TUNEL staining was carried out on retinal cryosections that had been post-fixed in ethanol:acetic acid (2:1) for 5 min at −20°C followed by two washes in PBS, 5 min each wash. Following manufacturer's instructions, the ApopTag® Fluorescein *In Situ* Apoptosis Detection Kit (Millipore) was used to detect levels of apoptotic cell death. For retinal and RPE flatmounts, the anterior segment of the eye was removed after fixation and then the retina dissected off the RPE/choroid in one sheet. Retinal tissue was blocked with 3%

non-fat dried milk and 0.3% Triton X-100 in PBS for 1 h, and incubated with primary antibodies or lectins according to manufacturer's instructions. RPE/choroid flatmounts were blocked with 5% bovine serum albumin and 0.5% Triton X-100 in PBS for 1 h, and incubated with zonula occludens-1 antibody alone or co-labeled with phalloidin. After incubation with secondary antibodies, retinal and RPE/choroid flatmounts were transferred to a microscope slide, small cuts were made in the tissue so that it could be flattened and then they were mounted using Fluoromount-G (Southern Biotech). All immunofluorescent images were acquired using a Zeiss 510 laser scanning confocal microscope. For cone and microglial flatmounts, the cell counts were averaged in six eyes from four areas in the superior, inferior, temporal and nasal retina ~0.5 mm from the center of the optic nerve using the ImageJ software.

Western blotting

Briefly, the neuroretina or RPE were snap frozen in liquid nitrogen and homogenized by sonication in lysis buffer [10 mM Tris–base, pH 7.4, 150 mM NaCl, 1 mM ethylenediaminetetraacetic acid (EDTA), 1 mM ethylene glycol tetraacetic acid (EGTA), 1% Triton X-100, 0.5% NP-40, protease and phosphatase inhibitor cocktail (Roche)]. Protein concentration was determined by the DC protein assay (Bio-Rad, Hercules, CA, USA). Proteins (40 μg) were separated by sodium dodecyl sulfate–polyacrylamide gel electrophoresis, transferred to Immobilon-FL membrane (Millipore), blocked in 5% non-fat milk powder in PBS/0.1% Tween 20 (PBST) for 2 h at RT and incubated overnight at 4°C with primary antibody in the same buffer and diluted according to manufacturer's instructions. Following three washes in PBST, the membrane was incubated in the dark for 1 h with a Li-COR secondary antibody (IRDye 800), washed three times in PBST in the dark and protein bands were visualized using a Li-COR Odyssey detector (Mandel Scientific). The NIH Image J software was used to quantify band intensities relative to β-actin loading controls.

Mitochondrial protein extraction

Retinal tissue was rinsed with ice-cold sucrose buffer containing 250 mM sucrose, 20 mM 4-(2-hydroxyethyl)-1-piperazineethanesulfonic acid, 1 mM EGTA, and 1 mM EDTA adjusted to pH 7.4 with potassium hydroxide. Cell extracts were obtained in ice-cold sucrose buffer supplemented with 1 mM dithiothreitol, 100 μM PMSF, 1 μg/ml chymostatin, 1 μg/ml leupeptin, 1 μg/ml antiparin and 1 μg/ml pepstatin A. Tissue lysates were homogenized by sonication and centrifuged (4°C) at 500*g* for 12 min to pellet the cell nuclei and cell debris. The supernatant (total fraction) was further centrifuged at 12 000*g* for 20 min. The resulting pellet (mitochondrial fraction) was resuspended in supplemented sucrose buffer and the samples were stored at −80°C until use. For immunoblotting 30 μg of mitochondrial proteins were used.

Intravitreal injections

Heterozygous pigmented P23H-1 rats were anesthetized with isoflurane, eyes were anesthetized with proparacaine hydrochloride (Alcon) and pupils were dilated with 1% tropicamide (Bausch and Lomb). Body temperature was maintained at 37°C by using a heating pad. Intravitreal injection was performed with a 31-gauge needle attached to a 10 μl Gastight Syringe (Hamilton). The tip of the needle was inserted 1.5 mm behind the corneal limbus, at an angle of 45° and caution was taken to avoid damaging the lens. The following procedure was carried out under a dual-headed ophthalmic surgical microscope (Zeiss). A 5 μl dose of P2RX7 inhibitor BBG (Santa Cruz Biotechnology) at the concentration of 300 nM dissolved in PBS was administered into one eye, and PBS vehicle was administered into the contralateral eye serving as the control. After 1-week post-injection rats were sacrificed and retinal tissue was collected.

LDH assay

Vitreous samples (10 μl) were surgically extracted from WT and P23H rats, and extracellular LDH activity (a marker for necrosis) was analyzed using an LDH Cytotoxicity Assay Kit (Pierce) according to the manufacturer's recommendations.

Semi-quantitative RT-PCR

Total RNA was extracted from tissues using Aurum™ Total RNA Mini Kit (Bio-Rad Laboratories) according to the manufacturer's recommendations. cDNA was amplified using QuantiTect Reverse Transcription Kit (Qiagen) and relative gene expression of *Hmgb1* (Rn02377062_g1), *Il-1α* (Rn00566700_m1), *Il-1β* (Rn00580432_m1), *Il-18* (Rn01422083_m1) and *Gapdh* (Rn01775763_g1) were quantified using a ViiA 7 Real-Time PCR system (Applied Biosystems). All reactions were performed using 5 ng of cDNA and the TaqMan Universal Master Mix (2X). FAM-labeled TaqMan gene expression assays were used for *Hmgb1*, *Il-1α*, *Il-1β* and *Il-18* whereas a VIC-labeled TaqMan assay was used for endogenous control *Gapdh*. Thermocycling parameters were as follows: 2 min at 50°C, 20 s at 95°C, 40 cycles of 1 s at 95°C, plus 20 s at 60°C. Real-time PCR data were analyzed by the comparative C_T method. Each reaction was undertaken on three independent occasions, and for each of these, individual samples were subdivided into three aliquots for measurement.

Electroretinography

Response of the retina to light flashes were recorded using an Espion E2 system with a Colordome mini-Ganzfeld stimulator (Diagnosys LLC). Dark-adapted responses were recorded at P21, P45, P90 and P120 by averaging 15 responses at a stimulus intensity of 3.16 cd s/m^2. Light-adapted cone responses were carried out in 30 cd/m^2 background light.

Enzyme-linked immunosorbent assay

The amount of carbonyl adducts of proteins in neuroretinal extracts was determined using the OxiSelect Protein Carbonyl enzyme-linked immunosorbent assay (ELISA) kit (Cell Biolabs, Inc.), according to manufacturer's instructions. ELISA was also used to quantify cytokines in the neuroretinal supernatants from the various experimental groups using the rat IL-1β kit (Abcam) according to the manufacturer's instructions. All ELISAs were conducted a minimum of three times in triplicate.

Statistics

Analyses were performed with GraphPad Prism 5.0. For parameter comparisons between groups, an unpaired two-tailed Student's *t*-test. *P*-values of <0.05 were considered significant. Multiple group comparison was performed by one-way or two-way ANOVA followed by Tukey–Kramer adjustments. Differences were considered significant at $P < 0.05$. Results are reported as mean ± SEM.

Supplementary Material

Supplementary Material is available at *HMG* online.

Acknowledgements

The authors acknowledge the use of the Wax-it Histology Service Facility, the Rodent Functional Testing Suite at the University of British Columbia, and Dr A. Gharhary for access to the Real-Time PCR facility.

Conflict of Interest statement. None declared.

Funding

This work was supported by the Canadian Institutes of Health Research Team grant (grant number: 222728 to K.G.E., C.G.E. and O.L.M.).

References

1. Kaushal, S., Ridge, K.D. and Khorana, H.G. (1994) Structure and function in rhodopsin: the role of asparagine-linked glycosylation. *Proc. Natl Acad. Sci. USA*, **91**, 4024–4028.
2. Liang, C.J., Yamashita, K., Muellenberg, C.G., Shichi, H. and Kobata, A. (1979) Structure of the carbohydrate moieties of bovine rhodopsin. *J. Biol. Chem.*, **254**, 6414–6418.
3. Sohocki, M.M., Daiger, S.P., Browne, S.J., Rodriguez, H., Northrup, J.R., Heckenlively, D.G., Birch, D.G., Mintz-Hittner, H., Ruiz, R.S., Lewis, R.A. *et al.* (2001) Prevalence of mutations causing retinitis pigmentosa and other inherited retinopathies. *Hum. Mutat.*, **17**, 42–51.
4. Hartong, D.T., Berson, E.L. and Dryja, T.P. (2006) Retinitis pigmentosa. *Lancet*, **368**, 1795–1809.
5. Berson, E.L. (1993) Retinitis pigmentosa. The Friedenwald lecture. *Invest. Ophthalmol. Vis. Sci.*, **34**, 1659–1676.
6. Saliba, R.S., Munro, P.M.G., Luthert, P.J. and Cheetham, M.E. (2002) The cellular fate of mutant rhodopsin: quality control, degradation and aggresome formation. *J. Cell Sci.*, **15**, 2907–2918.
7. Noorwez, S.M., Kuksa, V., Imanishi, Y., Zhu, L., Filipek, S., Palczewski, K. and Kaushal, S. (2003) Pharmacological chaperone-mediated in vivo folding and stabilization of the P23H-opsin mutant associated with autosomal dominant retinitis pigmentosa. *J. Biol. Chem.*, **278**, 14442–14450.
8. Kaur, J., Mencl, S., Sahaboglu, A., Farinelli, P., van Veen, T., Zrenner, E., Ekström, P., Paquet-Durand, F. and Arango-Gonzalez, B. (2011) Calpain and PARP activation during photoreceptor cell death in P23H and S334ter rhodopsin mutant rats. *PLoS One*, **6**, e22181.
9. Rana, T., Shinde, V.M., Starr, C.R., Kruglov, A.A., Boitet, E.R., Kotla, P., Zolotukhin, S., Gross, A.K. and Gorbatyuk, M.S. (2014) An activated unfolded protein response promotes retinal degeneration and triggers an inflammatory response in the mouse retina. *Cell Death Dis.*, **5**, e1578.
10. Muruve, D.A., Petrilli, V., Zaiss, A.K., White, L.R., Clark, S.R., Ross, P.J., Parks, R.J. and Tschopp, J. (2008) The inflammasome recognizes cytosolic microbial host DNA and triggers an innate immune response. *Nature*, **452**, 103–107.
11. Zhou, R., Yazdi, A.S., Menu, P. and Tschopp, J. (2011) A role for mitochondria in NLRP3 inflammasome activation. *Nature*, **469**, 221–225.
12. Allam, R., Darisipudi, M.N., Tschopp, J. and Anders, H.J. (2013) Histones trigger sterile inflammation by activating the NLRP3 inflammasome. *Eur. J. Immunol.*, **43**, 3336–3342.
13. Heid, M.E., Keyel, P.A., Kamga, C., Shiva, S., Watkins, S.C. and Salter, R.D. (2013) Mitochondrial reactive oxygen species induces NLRP3-dependent lysosomal damage and inflammasome activation. *J. Immunol.*, **191**, 5230–5238.
14. Bauernfeind, F.G., Horvath, G., Stutz, A., Alnemri, E.S., MacDonald, K., Speert, D., Fernandes-Alnemri, T., Wu, J., Monks, B.G., Fitzgerald, K.A. *et al.* (2009) Cutting edge: NF-kappaB activating pattern recognition and cytokine receptors license NLRP3 inflammasome activation by regulating NLRP3 expression. *J. Immunol.*, **183**, 787–791.
15. Schroder, K. and Tschopp, J. (2010) The inflammasomes. *Cell*, **140**, 821–832.
16. Rathinam, V.A., Vanajam, S.K. and Fitzgerald, K.A. (2012) Regulation of inflammasome signaling. *Nat. Immunol.*, **13**, 333–342.
17. Zhang, D.W., Shao, J., Lin, J., Zhang, N., Lu, B.J., Lin, S.C., Dong, M.Q. and Han, J. (2009) RIP3, an energy metabolism regulator that switches TNF-induced cell death from apoptosis to necrosis. *Science*, **325**, 332–336.
18. Cho, Y.S., Challa, S., Moquin, D., Genga, R., Ray, T.D., Guildford, M. and Chan, F.K. (2009) Phosphorylation-driven assembly of the RIP1-RIP3 complex regulates programmed necrosis and virus-induced inflammation. *Cell*, **137**, 1112–1123.
19. Yabal, M., Muller, N., Adler, H., Knies, N., Groß, C.J., Damagaard, R.B., Kanegane, H., Ringelhan, M., Kaufmann, T., Heikenwälder, M. *et al.* (2014) XIAP restricts TNF- and RIP3-dependent cell death and inflammasome activation. *Cell Rep.*, **7**, 1796–1808.
20. Ripps, H. (2002) Cell death in retinitis pigmentosa: gap junctions and the 'bystander' effect. *Exp. Eye Res.*, **74**, 327–336.
21. Arango-Gonzalez, B., Trifunović, D., Sahaboglu, A., Kranz, K., Michalakis, S., Farinelli, P., Koch, S., Koch, F., Cottet, S., Janssen-Bienhold, U. *et al.* (2014) Identification of a common non-apoptotic cell death mechanism in hereditary retinal degeneration. *PLoS One*, **9**, e112142.
22. Gregory-Evans, K., Fariss, R.N., Possin, D.E., Gregory-Evans, C. Y. and Milam, A.H. (1998) Abnormal cone synapses in human cone-rod dystrophy. *Ophthalmology*, **105**, 2306–2312.
23. Sizova, O.S., Shinde, V.M., Lenox, A.R. and Gorbatyuk, M.S. (2014) Modulation of cellular signaling pathways in P23H rhodopsin photoreceptors. *Cell Signal*, **26**, 665–672.
24. Yokoyama, T., Miyazawa, K. and Naito, M. (2008) Vitamin K2 induces autophagy and apoptosis simultaneously in leukemia cells. *Autophagy*, **4**, 629–640.
25. Chan, F.K., Moriwaki, K. and De Rosa, M.J. (2013) Detection of necrosis by release of lactate dehydrogenase activity. *Methods Mol. Biol.*, **979**, 65–70.
26. Acosta, M.L., Shin, Y.S., Ready, S., Fletcher, E.L., Christi, D.L. and Kalloniatis, M. (2010) Retinal metabolic state of the proline-23-histidine rat model of retinitis pigmentosa. *Am. J. Physiol. Cell Physiol.*, **298**, 764–774.
27. Wang, Z., Jiang, H., Chen, S., Du, F. and Wang, X. (2012) The mitochondrial phosphatase PGAM5 functions at the convergence points of multiple necrotic cell death pathways. *Cell*, **148**, 228–243.
28. Santos, A., Humayun, M.S., de Juan, E. Jr, Greenburg, R.J., Marsh, M.J., Klock, I.B. and Milam, A.H. (1997) Preservation of the inner retina in retinitis pigmentosa. A morphometric analysis. *Arch. Ophthalmol.*, **115**, 511–515.
29. Strettoi, E., Porciatti, V., Falsini, B., Pignatelli, V. and Rossi, C. (2002) Morphological and functional abnormalities in the inner retina of the rd/rd mouse. *J. Neurosci.*, **22**, 5492–5504.
30. Rivera, S.C., Sitaras, N., Noueihed, B., Hamel, D., Madaan, A., Zhou, T., Honore, J.C., Quiniou, C., Joyal, J.S., Hardy, P. *et al.* (2013) Microglia and interleukin-1β in ischemic retinopathy elicit microvascular degeneration through neuronal semaphorin-3A. *Arterioscler. Thromb. Vasc. Biol.*, **33**, 1881–1891.

31. Krady, J.K., Basu, A., Allen, C.M., Xu, Y., LaNoue, K.F., Gardner, T.W. and Levison, S.W. (2005) Minocycline reduces proinflammatory cytokine expression, microglial activation, and caspase-3 activation in a rodent model of diabetic retinopathy. *Diabetes*, **54**, 1559–1565.
32. Tarallo, V., Hirano, Y., Gelfand, B.D., Dridi, S., Kerur, N., Kim, Y., Cho, W.G., Kaneko, H., Fowler, B.J., Bogdanovich, S. *et al.* (2012) DICER1 loss and Alu RNA induce age-related macular degeneration via the NLRP3 inflammasome and MyD88. *Cell*, **149**, 847–859.
33. Machida, S., Kondo, M., Jamison, J.A., Khan, N.W., Kononen, L.T., Sugawara, T., Bush, R.A. and Sieving, P.A. (2000) P23H rhodopsin transgenic rat: correlation of retinal function with histopathology. *Invest. Ophthalmol. Vis. Sci.*, **41**, 3200–3209.
34. Murakami, Y., Matsumoto, H., Roh, M., Suzuki, J., Hisatomi, Y., Ikeda, Y., Miller, J.W. and Vavvas, D.G. (2012) Receptor interacting protein kinase mediates necrotic cone but not rod cell death in a mouse model of inherited degeneration. *Proc. Natl Acad. Sci. USA*, **109**, 14598–14603.
35. Ofengeim, D. and Yuan, J. (2013) Regulation of RIP1 kinase signalling at the crossroads of inflammation and cell death. *Nat. Rev. Mol. Cell Biol.*, **14**, 727–736.
36. Lukens, J.R., Vogel, P., Jordan, G.R., Kelliher, M.A., Iwakura, Y., Lamkanfi, M. and Kanneganti, T.D. (2013) RIP-1 driven autoinflammation targets IL-1α independently of inflammasomes and RIP3. *Nature*, **498**, 224–227.
37. Levine, R.L., Williams, J.A., Stadtman, E.R. and Shacter, E. (1994) Carbonyl assays for determination of oxidatively modified proteins. *Methods Enzymol.*, **233**, 346–357.
38. Liu, Y., Yao, W., Xu, J., Qiu, Y., Cao, F., Li, S., Yang, S., Yang, H., Wu, Z. and Hou, Y. (2015) The anti-inflammatory effects of acetoaminophen and N-acetylcysteine through suppression of the NLRP3 inflammasome pathway in LPS-challenged piglet mononuclear phagocytes. *Innate Immun.*, **21**, 587–597.
39. Cruz, C.M., Rinna, A., Forman, H.J., Ventura, A.L., Persechini, P.M. and Ojcius, D.M. (2007) ATP activates a reactive oxygen species-dependent oxidative stress response and secretion of proinflammatory cytokines in macrophages. *J. Biol. Chem.*, **282**, 2871–2879.
40. Bartlett, R., Yerbury, J.J. and Sluyter, R. (2013) P2X7 receptor activation induces reactive oxygen species formation and cell death in murine EOC13 microglia. *Mediators Inflamm.*, **271813**, doi:10.1155/2013/271813.
41. Peng, W., Cotrina, M.L., Han, X., Yu, H., Bekar, L., Blum, L., Takano, T., Tian, G.F., Goldman, S.A. and Nedergaard, M. (2009) Systemic administration of an antagonist of the ATP-sensitive receptor P2X7 improves recovery after spinal cord injury. *Proc. Natl Acad. Sci. USA*, **106**, 12489–12493.
42. Khakh, B.S. and North, R.A. (2006) P2X receptors as cell-surface ATP sensors in health and disease. *Nature*, **442**, 527–532.
43. Sangiuliano, B., Perez, N.M., Moreira, D.F. and Belizario, J.E. (2014) Cell death associated molecular-pattern molecules: inflammatory signaling and control. *Mediators Inflamm.*, **821043**, doi:10.1155/2014/821043.
44. Sakami, S., Maeda, T., Bereta, G., Okano, K., Golczak, M., Sumaroka, A., Roman, A.J., Cideciyan, A.V., Jacobson, S.G. and Palczewski, K. (2011) Probing mechanisms of photoreceptor degeneration in a new mouse model of the common form of autosomal dominant retinitis pigmentosa due to P23H opsin mutations. *J. Biol. Chem.*, **286**, 10551–10567.
45. Kovarova, M., Hesker, P.R., Jania, L., Nguyen, M., Snouwaert, J.N., Xiang, X., Lommatzsch, S.E., Huang, M.T., Ting, J.P. and Koller, B.H. (2012) NLRP1-dependent pyroptosis leads to acute lung injury and morbidity in mice. *J. Immunol.*, **189**, 2006–2016.
46. Bhatt, L., Groeger, G., McDermott, K. and Cotter, T.G. (2010) Rod and cone photoreceptor cells produce ROS in response to stress in a live retinal explant system. *Mol. Vis.*, **16**, 283–293.
47. Tam, B.M. and Moritz, O.L. (2006) Characterization of rhodopsin P23H-induced retinal degeneration in a Xenopus laevis model of retinitis pigmentosa. *Invest. Ophthalmol. Vis. Sci.*, **47**, 3234–3241.
48. Kroeger, H., Messah, C., Ahern, K., Gee, J., Joseph, V., Matthes, M.T., Yasumura, D., Gorbatyuk, M.S., Chiang, W.C., LaVail, M.M. *et al.* (2012) Induction of endoplasmic reticulum stress genes, BiP and chop, in genetic and environmental models of retinal degeneration. *Invest. Ophthalmol. Vis. Sci.*, **53**, 7590–7599.
49. Chiang, W.C., Kroeger, H., Sakami, S., Messah, C., Yasumura, D., Matthes, M.T., Coppinger, J.A., Palczewski, K., LaVail, M.M. and Lin, J.H. (2015) Robust endoplasmic reticulum-associated degradation of rhodopsin precedes retinal degeneration. *Mol. Neurobiol.*, **52**, 679–695.
50. Lin, J.H., Li, H., Yasumura, D., Cohen, H.R., Zhang, C., Panning, B., Shokat, K.M., Lavail, M.M. and Walter, P. (2007) IRE1 signaling affects cell fate during the unfolded protein response. *Science*, **318**, 944–949.
51. Mendes, H.F. and Cheetham, M.E. (2008) Pharmacological manipulation of gain-of-function and dominant-negative mechanisms in rhodopsin retinitis pigmentosa. *Hum. Mol. Genet.*, **17**, 3043–3054.
52. Tam, B.M. and Moritz, O.L. (2007) Dark rearing rescues P23H rhodopsin-induced retinal degeneration in a transgenic Xenopus laevis model of retinitis pigmentosa: a chromophore-dependent mechanism characterized by production of N-terminally truncated mutant rhodopsin. *J. Neurosci.*, **27**, 9043–9053.
53. Tam, B.M., Qazalbash, A., Lee, H.C. and Moritz, O.L. (2010) The dependence of retinal degeneration caused by the rhodopsin P23H mutation on light exposure and vitamin a deprivation. *Invest. Ophthalmol. Vis. Sci.*, **51**, 1327–1334.
54. Gorbatyuk, M.S., Knox, T., LaVail, M.M., Gorbatyuk, O.S., Noorwez, S.M., Hauswirth, W.W., Lin, J.H., Muzyczka, N. and Lewin, A.S. (2010) Restoration of visual function in P23H rhodopsin transgenic rats by gene delivery of BiP/Grp78. *Proc. Natl Acad. Sci. USA*, **107**, 5961–5966.
55. Vanlangenakker, N., Vanden Berghe, T., Krysko, D.V., Festjens, N. and Vandenabeele, P. (2008) Molecular mechanisms and pathophysiology of necrotic cell death. *Curr. Mol. Med.*, **8**, 207–220.
56. Murakami, Y., Matsumoto, H., Roh, M., Giani, A., Kataoka, K., Morizane, Y., Kayama, M., Thanos, A., Nakatake, S., Hisatomi, T. *et al.* (2014) Programmed necrosis, not apoptosis, is a key mediator of cell loss and DMAP-mediated inflammation in dsRNA-induced retinal degeneration. *Cell Death Differ.*, **21**, 270–277.
57. Matsumoto, H., Kataoka, K., Tsoka, P., Connor, K.M., Miller, J.W. and Vavvas, D.G. (2014) Strain difference in photoreceptor cell death after retinal detachment in mice. *Invest. Ophthalmol. Vis. Sci.*, **55**, 4165–4174.
58. Rosenbaum, D.M., Degterev, A., David, J., Rosenbaum, P.S., Roth, S., Grotta, J.C., Cuny, G.D., Yuan, J. and Savitz, S.I. (2010) Necroptosis, a novel form of caspase-independent cell death, contributes to neuronal damage in a retinal ischemia-reperfusion injury model. *J. Neurosci. Res.*, **88**, 1569–1576.
59. Komeima, K., Rogers, B.S. and Campochiaro, P.A. (2007) Antioxidants slow photoreceptor cell death in mouse models of retinitis pigmentosa. *J. Cell Physiol.*, **213**, 809–815.

60. Byrne, L.C., Dalkara, D., Luna, G., Fisher, S.K., Clerin, E., Sahal, J.A., Léveillard, T. and Flannery, J.G. (2015) Viral-mediated RdCVF and RdCVFL expression protects cone and rod photoreceptors in retinal degeneration. *J. Clin. Invest.*, **125**, 105–116.
61. Punzo, C., Kornacker, K. and Cepko, C.L. (2009) Stimulation of the insulin/mTOR pathway delays cone death in a mouse model of retinitis pigmentosa. *Nat. Neurosci.*, **12**, 44–52.
62. Gupta, N., Brown, K.E. and Milam, A.H. (2003) Activated microglia in human retinitis pigmentosa, late onset retinal degeneration, and age-related macular degeneration. *Exp. Eye Res.*, **76**, 463–471.
63. Kerur, N., Hirano, Y., Tarallo, V., Fowler, B.J., Bastos-Carvalho, A., Yasuma, T., Yasuma, R., Kim, Y., Hinton, D.R., Kirschning, C.J. *et al.* (2013) TLR-independent and P2X7-dependent signaling mediate *Alu* RNA-induced NLRP3 inflammasome activation in geographic atrophy. *Invest. Ophthalmol. Vis. Sci.*, **54**, 7395–7401.
64. Guerra, A.N., Gavala, M.L., Chung, H.S. and Bertics, P.J. (2007) Nucleotide receptor signalling and the generation of reactive oxygen species. *Purinerg. Signal*, **3**, 39–51.
65. Heneka, M.T., Krummer, M.P., Stutz, A., Delekate, A., Schwartz, S., Vieira-Saecker, A., Griep, A., Axt, D., Remus, A., Tzeng, T.C. *et al.* (2013) NLRP3 is activated in Alzheimer's disease and contributes to pathology in APP/PS1 mice. *Nature*, **493**, 674–678.
66. Yoshida, N., Ikeda, Y., Notomi, S., Ishikawa, K., Murakami, Y., Hisatomi, T., Enaida, H. and Ishibashi, T. (2013) Clinical evidence of sustained chronic inflammatory reaction in retinitis pigmentosa. *Ophthalmology*, **120**, 100–105.
67. Noailles, A., Fernandez-Sanchez, L., Lax, P. and Cuenca, N. (2014) Microglia activation in a model of retinal degeneration and TUDCA neuroprotective effects. *J. Neuroinflamm.*, **11**, e186.
68. Lee, S.Y., Usui, S., Zafar, A.B., Ovenson, B.C., Jo, Y.J., Lu, L., Masoudi, S. and Campochiaro, P.A. (2011) N-Acetylcysteine promotes long-term survival of cones in a model of retinitis pigmentosa. *J. Cell Physiol.*, **226**, 1843–1849.
69. Sato, K., Li, S., Gordon, W.C., He, J., Liou, G.I., Hill, J.M., Travis, G.H., Bazan, N.G. and Jin, M. (2013) Receptor interacting protein kinase-mediated necrosis contributes to cone and rod photoreceptor degeneration in the retina lacking interphotoreceptor retinoid-binding protein. *J. Neurosci.*, **33**, 17458–17468.
70. Leonard, K.C., Petrin, D., Copeland, S.G., Baker, A.N., Leonard, B.C., LaCasse, E.C., Hauswirth, W.W., Korneluk, R.G. and Tsilfidis, C. (2007) XIAP protection of photoreceptors in animal models of retinitis pigmentosa. *PLoS One*, **3**, e3314.
71. Parfitt, D.A., Aguila, M., McCulley, C.H., Bevilacqua, D., Mendes, H.F., Athanasiou, D., Novoselov, S.S., Kanuga, N., Munro, P.M., Coffey, P.J. *et al.* (2014) The heat-shock response co-inducer arimoclomol protects against retinal degeneration in rhodopsin retinitis pigmentosa. *Cell Death Dis.*, **5**, e1236.
72. Adekeye, A., Haeri, M., Solessio, S. and Knox, B.E. (2014) Ablation of the proapoptotic genes CHOP or Ask1 does not prevent or delay loss of visual function in a P23H transgenic mouse model of retinitis pigmentosa. *PLoS One*, **9**, e83871.
73. Ghosh, R., Wang, L., Wang, E.S., Perera, B.G., Igbaria, A., Morita, S., Prado, K., Thamsen, M., Caswell, D., Macias, H. *et al.* (2014) Allosteric inhibition of the IRE1α RNase preserves cell viability and function during endoplasmic reticulum stress. *Cell*, **158**, 534–548.
74. Talcott, K.E., Ratnam, K., Sundquist, S.M., Lucero, A.S., Lujan, B.J., Tao, W., Porco, T.C., Roorda, A. and Duncan, J.L. (2011) Longitudinal study of cone photoreceptors during retinal degeneration and in response to ciliary neurotrophic factor treatment. *Invest. Ophthalmol. Vis. Sci.*, **52**, 2219–2226.
75. Cusato, K., Bosco, A., Rozental, R., Guimaraes, C.A., Reese, B. E., Linden, R. and Spray, D.C. (2003) Gap junctions mediate bystander cell death in developing retina. *J. Neurosci.*, **23**, 6413–6422.
76. Pozner, R.G., Ure, A.E., Jaquenod de Giusti, C., D'Atri, L.P., Italiano, J.E., Torres, O., Romanowski, V., Schattner, M. and Gómez, R.M. (2010) Junín virus infection of human hematopoietic progenitors impairs in vitro proplatelet formation and platelet release via a bystander effect involving type I IFN signaling. *PLoS Pathog.*, **6**, e1000847.
77. Frantseva, M.V., Kokarovtseva, L., Naus, C.G., Carlen, P.L., MacFabe, D. and Perez- Velazquez, J.L. (2002) Specific gap junctions enhance the neuronal vulnerability to brain traumatic injury. *J. Neurosci.*, **22**, 644–653.
78. Dunn, H.C., Ager, R.R., Baglietto-Vargas, D., Cheng, D., Kitazawa, M., Cribbs, D.H. and Medeiros, R. (2015) Restoration of lipoxin A4 signaling reduces Alzheimer's disease-like pathology in the 3xTg-AD mouse model. *J. Alzheimers Dis.*, **43**, 893–903.
79. Mesnil, M., Piccoli, C., Tiraby, G., Willecke, K. and Yamasaki, H. (1996) Bystander killing of cancer cells by herpes simplex virus thymidine kinase gene is mediated by connexins. *Proc. Natl Acad. Sci. USA*, **93**, 1831–1835.